NASA Technical Memorandum 109181

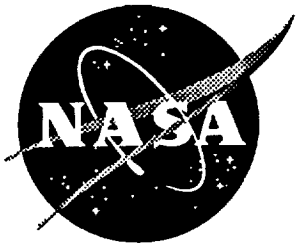

DSMC Calculations for a 70° Blunted Cone at 3.2 km/s in Nitrogen

J. N. Moss and J. M. Price
Langley Research Center, Hampton, Virginia

V. K. Dogra
ViGYAN, Inc., Hampton, Virginia

January 1995

National Aeronautics and
Space Administration
Langley Research Center
Hampton, Virginia 23681-0001

DSMC Calculations for a 70° Blunted Cone at 3.2 km/s in Nitrogen

James N. Moss and Joseph M. Price
NASA Langley Research Center
Hampton, VA 23681-0001

and

Virendra K. Dogra
ViGYAN, Inc.
Hampton, VA

Abstract

Numerical results obtained with the direct simulation Monte Carlo (DSMC) method are presented for Mach 15.6 nitrogen flow about a 70-deg spherically blunted cone at zero incidence. This flow condition is one of several generated in the Large Energy National Shock (LENS) tunnel during tests of a 15.24 cm diameter model with an afterbody sting. The freestream Knudsen number, based on model diameter, is 0.0023. The focus of the DSMC calculations is to characterize the near wake flow under conditions where rarefaction effects may influence afterbody aerothermal loads. This report provides information concerning computational details along with flowfield and surface quantities. Calculations show that the flow enveloping the test model is in thermal nonequilibrium and a sizable vortex develops in the near wake. Along the model baseplane the heating rates are about 0.6 percent of the forebody stagnation value while the maximum heating along the sting is about 4.2 percent of the forebody stagnation value. Comparison of a Navier-Stokes solution with the present calculations show good agreement for surface heating, pressure, and skin friction results.

Nomenclature

A	base area of cone, $A = \pi d^2/4$
C_D	drag coefficient, $C_D = 2D/\rho_\infty V_\infty^2 A$
C_f	skin friction coefficient, $C_f = 2\tau/\rho_\infty V_\infty^2$
C_H	heat transfer coefficient, $C_H = 2q/\rho_\infty V_\infty^3$
C_p	pressure coefficient, $C_p = 2p/\rho_\infty V_\infty^2$
d	base diameter
dref	molecular diameter at reference temperature
D	drag
Kn	Knudsen number, $Kn = \lambda/d$
M	Mach number
$\overline{M}$	molecular weight, of N_2, $\overline{M}$ = 28.02 g/mole
p	surface pressure
q	surface heat flux
R	gas constant for N_2, R = 296.7 J/kgK
R_b	cone base radius
R_c	corner radius
R_n	nose radius
Re_d	Reynolds number, $Re_d = \rho V d/\mu$
s	distance along the body surface measured from the stagnation point
$\bar{s}$	temperature exponent of the coefficient of viscosity
S	speed ratio, $S = V\sqrt{\overline{M}/2RT}$
T	thermodynamic temperature
T_i	internal kinetic temperature
T_{ov}	overall kinetic temperature
T_r	rotational temperature

T_t	translational temperature
T_v	vibrational temperature
T_w	surface temperature
u	axial velocity
v	radial velocity
V	velocity
x	axial distance from stagnation point measured along symmetry axis
y	radial distance from symmetry axis
γ	ratio of specific heats
Γ	Gamma function
λ	mean free path
μ	dynamic viscosity
ρ	density
σ	collision cross section
τ	shear stress

Subscripts

ref	reference value
w	surface values
∞	freestream values

Introduction

In order to reduce design uncertainties for hypersonic vehicles, it has and continues to be a fundamental tenant that experiments be performed to aid in the development and testing of computational models with regard to key fluid dynamic and thermochemical processes. Computational tools that successfully meet these tests can then be applied with higher confidence to flight environments for which it may be

impossible to duplicate in ground-based facilities. The current study is part of such a process where the focus is hypersonic wake flows produced by a 70-deg spherically blunted cone; the same forebody configuration as that for the Mars Pathfinder Probe. The blunt body/wake flow problem is only one of several fundamental hypersonic problems being addressed both computationally and experimentally under the aegis[1] of AGARD Working Group 18. The emphasis of the AGARD blunt body/wake studies is the significance of rarefaction and real gas effects on the near wake as it influences the afterbody heating and pressure distributions. Experiments are being conducted in both low density wind tunnels and impulse tunnels. Computations are being made with direct simulation Monte Carlo (DSMC) and Navier Stokes methods for selected experimental[2-8] cases and generic flight conditions[9-11].

The present focus is the application of the DSMC method of Bird[12-13] to one set of test conditions that have been run in the Large Energy National Shock Tunnel (LENS) facility[14-15]. The model was a 70°spherically blunted cone with a 0.1524 m base diameter and sting mounted at zero incidence. For the low Reynolds number test ($Re_{\infty,d}$=8,193) made in Mach 15.6 nitrogen, the flow energy was approximately 5 MJ/kg. Such a flow provides a relatively simple yet important test condition in that there is significant thermal nonequilibrium but negligible dissociation. Measurements included surface heating rates and pressure along the forebody, base plane, and sting with heating instrumentation concentrated along the sting. (The experimental data are to be released[16] at a later date.) The present paper describes the flowfield and surface results obtained with the DSMC simulations and the surface results are compared with those obtained using a Navier Stokes solver.

Computational Method and Boundary Conditions

The direct simulation Monte Carlo (DSMC) method[12-13] provides a numerical capability that acknowledges the discrete nature of a gas and thereby provides a

capability of simulating flows across the complete flow spectrum of continuum to free molecular flows. However, the DSMC method is normally applied to the transitional and free molecular flow regimes since the computing requirements can become excessive for continuum applications.

The model configuration and computational grid are shown in Figs. 1 and 2, respectively. The computational domain is such that the upstream and side boundaries can be specified as freestream conditions. The downstream outflow boundary is specified as a vacuum condition located (0.4 m) downstream of the forebody stagnation point. (The model with sting is 0.489 m in length; however, a support is affixed to the end of the sting. This support was not modeled in the present study.) Figure 1 presents information concerning model configuration and Fig. 2 shows the physical extent of the computational domain which is subdivided into 15 unstructured regions with each region subdivided into computational cells for a total of 22,808 cells. The number of cells shown in Fig. 2(a) have been reduced for clarity (one-fourth the number normal to the surface and one-half along the surface). The number of simulated molecules is of the order of 20 per cell. Within a given region, each simulated molecule represents a fixed number of physical or real molecules (a large number on the order of 1.0×10^{11}).

The molecular collisions are simulated using the variable hard sphere (VHS) molecular model. This model employs the simple hard sphere angular scattering law so that all directions are equally possible for post-collision velocity in the center-of-mass frame of reference. However, the collision cross section is a function of the relative energy in the collision. The freestream viscosity and mean free path are evaluated using the VHS collision model with $T_{ref} = 300$ K, $d_{ref} = 4.07 \times 10^{-10}$m and $\bar{s} = 0.75$ (d_{ref} is the molecular diameter at reference temperature T_{ref} and $\bar{s}$ is the temperature exponent of the coefficient of viscosity). The freestream mean free path is calculated from the relation (see Ref. 12).

$$\lambda_\infty = \frac{(T_\infty/T_{ref})^\omega}{[\sqrt{2}n_\infty \sigma_{ref} (2-\omega)^\omega \Gamma (2-\omega)]} \quad (1)$$

$$\omega = \bar{s} - 1/2 \quad (2)$$

Energy exchange between kinetic and internal modes is controlled by the Larsen-Borgnakke[17] statistical model. For the present study, simulations are performed using a nonreacting gas model with one chemical species (N_2) while considering energy exchange between translational, rotational, and vibrational modes (rotational relaxation collision number of 5 and vibrational relaxation collision number a function of the cell translational temperature using the functional relation and constants given in Appendix A of Ref. 12).

Several preliminary runs were made to adjust the cell resolution near the surface such that the cell dimension normal to the surface was less than the local mean free path. This was achieved except for the base plane where some of the cells had a thickness equal to 1.5 λ.

Freestream and Surface Conditions

The freestream nitrogen flow is assumed to be uniform at the specified[16] test conditions. Also, the freestream is assumed to be in thermal equilibrium; however, this is problematic due to the nozzle expansion. Specific inputs for the DSMC simulation are:

$$V_\infty = 3245.8 \text{ m/s}$$

$$n_\infty = 2.807 \times 10^{21} \text{ m}^{-3}$$

$$T_\infty = 103.7 \text{ K}$$

Other quantities of interest are:

$$\rho_\infty = 1.306 \times 10^{-4} \text{ kg/m}^3$$

$$p_\infty = 4.02 \text{ N/m}^2$$

$M_\infty = 15.64$

$\lambda_\infty = 0.35$ mm

$\mu_\infty = 7.88 \times 10\text{-}6$ Pa•s

$Re_{\infty,d} = 8, 193$

$Kn_\infty = 0.0023$

where the viscosity and mean free path were evaluated with the variable hard sphere collision model and the characteristic length is the model base diameter (d = 0.1524 m). The surface temperature is assumed to be constant at 294.4 K and the gas-surface interaction model is diffuse with full thermal accommodation.

Simulation Details and Tabulated Results

Data presented are time averaged results obtained between time steps 59,533 and 81,333. Flowfield quantities were sampled every fifth time step. The simulation was not time consistent since the computational time step, in general, varied from region to region. Table 1 provides timing information for each of the 15 regions as to the time at which the time averaging was initiated ("FROM TIME") to the time where the sampling was terminated ("TO TIME"). Magnitudes of the time steps ranged from 3 ns (regions 4 and 8) to 225 ns (regions 14 and 15). Table 1 also presents a summary of the freestream conditions and various nondimensional parameters along with a listing of surface coordinates (midpoint of surface element), pressure, skin friction, incident heat flux, reflected heat flux, net heat flux, and the number of simulated nitrogen molecules that have impacted the surface elements during the time averaging interval. The next grouping of information includes the wetted distance from the forebody stagnation point to each surface element centroid (s/R_n) along with surface coefficients for pressure, skin friction, and heat transfer. The final data included in Table 1 is information concerning drag due to friction and pressure. The calculated axial force for the model is 19.77 N, producing a drag coefficient, C_D, of 1.58. The drag is dominated

by the pressure forces, comprising 97.9 percent of the total force. The stagnation heat transfer coefficient, C_H, has a value of 0.144.

Results and Discussion

Results of the present calculations are presented with emphasis on the wake flow structure and surface quantities. Then comparisons are made with the surface data obtained by Hash[18] using a Navier Stokes code.

Surface Results

Surface distributions for heating rate, pressure (normal force per unit area) and tangential shear stress are presented in Figs. 3 through 5. These data are presented as a function of nondimensional distance (s/R_n) along the surface measured from the forebody stagnation point. The flow expansion about the corner produces orders of magnitude reductions in surface quantities with respect to their forebody values. (The semilog plots [Figs. 3(b) and 4(b)] give a better perspective of the magnitude of heating and pressure along the base plane and sting.) Along the base plane, the heating is 2 orders of magnitude less than the forebody stagnation point value with a magnitude of about 0.2 W/cm^2 (0.6 percent of the stagnation value). The heating along the sting increases to a maximum value of about 1.3 W/cm^2 or about 4.2 percent of the forebody stagnation value at an s/R_n location of 8.4 ($x = 0.21$ m). Because of the low Reynolds number test condition, there is no evidence of a distinct shear layer impingement along the sting. That is, the surface heating rate increases with distance downstream of the base plane, reaches a maximum and then decreases gradually. Qualitative features for the pressure distribution are similar to those for heating rate with the pressure along the sting obtaining a maximum at the same location as that for heating. The skin friction experiences a maximum (Fig. 5) near the beginning of the outer corner expansion. Reattachment of the wake vortex along the sting (Fig. 5) is indicative of a thick shear

layer since the reattachment occurs at an s/R_n value of 6 (x = 0.121 m), about 9 cm upstream of the location of maximum heating and pressure.

Flow Structure

Some of the features of the forebody flow are depicted in Figs. 6 and 7 where the stagnation streamline values for density and temperature are shown, respectively. Evident is a distinct yet thick shock. Also, the temperature profiles indicate a significant degree of thermal nonequilibrium for the internal energy exchange models utilized in the current study. Unpublished calculations by the present authors for flow conditions similar to the present test case have shown the forebody flow structure to be noticeably altered while the surface heating to be insensitive to significant variations in the vibrational relaxation model.

The overall flowfield structure is highlighted in Figs. 8 through 17. As evidenced by the streamline contours (Fig. 8), a vortex develops for this test condition, extending a distance downstream of the base plane equal to 9 cm. Separation occurs on the outer corner (see Fig. 5, just before location 4) before the surface becomes tangent to the base plane. The minimum values for surface pressure and heating rate occur at or near this location. As discussed in Ref. 2, this minimum becomes more pronounced with increasing rarefaction. An indication of the extent of rarefaction is the magnitude of the velocity slip which is small for the present test case. Figure 9 provides such an indication where the cell average results (cell thickness < 0.5 λ) is presented for the axial velocity adjacent to the sting. Another measure of the wake structure is the sonic line location, and Fig. 10 presents this information along with other selected contours. Velocity vectors in the near wake are displayed in Fig. 11.

The density (Fig. 12) in the near wake has a minimum value near the junction of outer corner and base plane with magnitude of about 20 percent of the freestream. Density profiles normal to the sting are presented in Fig. 13 showing the profiles at three locations downstream of the base plane which is located at x = 0.0318m.

An overall perspective of the bow shock strength along with the expansion and recompression in the near wake is given by the "pressure-like' contour plot of Fig. 14. The "pressure-like" contours are the product of the local density and overall kinetic temperature normalized by the freestream value. "Pressure-like" profiles normal to the sting are presented in Fig. 15.

The extent of thermal nonequilibrium can be deduced from the contour plots of Figs. 16(a) through 16(d) where the overall kinetic temperature, T_{ov}, (defined for a nonequilibrium gas as the weighted mean of the translational and internal temperatures) translational temperature, rotational temperature, and vibrational temperature are presented, respectively. The entire flow domain is in thermal nonequilibrium. Along the forebody or compression region, the rotational and translational temperatures are in close agreement. As the flow expands into the near wake region, the rotational temperature is slightly greater than the corresponding translational value for most of the inner portion of the wake. The major difference is due to the slow excitation of the vibrational mode. A clearer indication of thermal nonequilibrium for the wake is presented in Fig. 17(a) where profiles of the difference in translational and internal temperatures normalized by the overall temperature are displayed. Small values for temperature jump and velocity slip are clearly evident along the sting as shown in Figs. 17(b) and 17(c).

Comparison of DSMC and Navier-Stokes Results

Figures 18 through 20 present comparisons of calculated surface quantities for heating rate, pressure, and skin friction. The current DSMC results are compared with predictions obtained by Hash[18] using an implicit, 3-temperature Navier Stokes solver[19]. The slip boundary conditions used are those discussed in Ref. 20. The overall agreement is shown to be good, particularly along the sting. Largest differences occur along the base plane. The implication of the present comparisons is that a Navier Stokes

solver can provide an adequate prediction of surface quantities for the current test problem.

Concluding Remarks

This report provides computational data characterizing the forebody and wake flow about a blunt axisymmetric configuration with an afterbody sting. Specifically, the forebody configuration is that for the Mars Pathfinder mission: a 70° spherically blunted cone. Furthermore, this configuration has been selected for the blunt body wake flow studies being addressed computationally and experimentally under the aegis of AGARD Working Group 18. The present study focuses on one of several shock tunnel conditions for which experiments have been performed in the LENS tunnel. The test gas is nitrogen. Future opportunities will exist for direct comparisons with the experimental data.

The current test condition provides a valuable complement to the flow conditions that can be produced in low-density wind tunnels in that more energetic flows are produced. For the current condition, high temperature gas effects are present. That is, the nitrogen gas that envelopes the test model is in thermal nonequilibrium, yet there is negligible dissociation. Absence of dissociation simplifies the characterization of heat transfer measurements in that there are no catalytic wall issues involved. However, specification of facility flow conditions are somewhat problematic because of the nonequilibrium nozzle expansion.

Results of the present DSMC calculations show a large vortex in the near wake region. The reattachment along the afterbody sting indicates a thick separated shear layer in that the location of maximum heating and pressure along the sting occurs about 9 cm downstream of the reattachment location. The heating rates along the base plane are about 2 orders of magnitude less than the forebody stagnation point value. Along the sting, the maximum heating rate is about 4.2 percent of the forebody stagnation

value. An independant calculation using the Navier-Stokes methodology yields good agreement with the DSMC results for surface heating, pressure, and skin friction.

If nonintrusive measurement techniques could be employed to characterize the thermal and chemical state of the gas species, valuable data would be obtained for developing and validating energy exchange and chemical reaction models for both compressive and expanding flows. By developing a test matrix that brackets the present level of rarefaction, using both nitrogen and air as test gases, and generating flow energies of 5 MJ/kg and higher, a number of valuable test conditions are possible with existing impulse facilities. Such a matrix of test conditions provides a wide spectrum of flows with both thermal and thermochemical nonequilibrium conditions.

References

[1]Anon: Hypersonic Experimental and Computational Capabilities: Improvement and Validation. AGARD AR-319, to be published in 1995.

[2]Moss, J. N., Mitcheltree, R. A., Dogra, V. K., and Wilmoth, R. G.: Direct Simulation Monte Carlo and Navier Stokes Simulations of Blunt Body Wake Flows," AIAA Journal, Vol. 32, No. 7, pp. 1399-1406, 1994.

[3]Moss, J. N., Dogra, V. K., and Wilmoth, R. G.: "DSMC Simulations of Mach 20 Nitrogen Flows about a 70° Blunted Cone and its Wake," NASA TM 107762, August 1993.

[4]Wilmoth, R. G., Mitcheltree, R. A., Moss, J. N., and Dogra, V. K.: "Zonally Decoupled DSMC Solutions of Hypersonic Blunt Wake Flows," AIAA Paper 93-2808, July 1993.

[5]Gilmore, M. R., Owen, A. K., and Jones, T. V.: "70° Aerobrake Vehicle Plus Afterbody in Hypersonic Rarefied Nitrogen Flow." Presented at the 19th International Symposium on Rarefied Gas Dynamics, Oxford, England, July 25-29, 1994.

[6]Gallis, M. A. and Harvey, J. K.: "Validation of DSMC Computations for the Flow Field Around a 70° Blunted Cone." Presented at the 19th International symposium on Rarefied Gas Dynamics, Oxford, England, July 25-29, 1994.

[7]Marriott, P. M. and Bartel, T. J.: "Comparison of DSMC Flow Field Predictions Using Different Models for Energy Exchange and Chemical Reaction Probability." Presented at the 19th International Symposium on Rarefied Gas Dynamics, Oxford, England, July 25-29, 1994.

[8]Chpoun, A., Cohen, L., Lengrand, J. C., Allegre, J., and Raffin, M.: "Numerical and Experimental Investigation of Rarefied Hypersonic Flow About an ASTV Re-entry Body." Paper presented at the 2nd European Computational Fluid Dynamics Conference, University of Stuttgart, Germany, Sept. 5-8, 1994

[9]Dogra, V. K., Moss, J. N., Wilmoth R. G., Taylor, J. C., and Hassan, H. A.: "Effects of Chemistry on Blunt Body Wake Structure," AIAA Paper 94-0352, January 1994.

[10]Yigiter, O: "Simulation of Two-Dimensional Rarefied Hypersonic Flows Using the Direct Simulation Monte Carlo Method." M.S. Thesis, supervised by M. C. Celenligil, Middle East Technical University, Ankara, Turkey, August 1994.

[11]Celenligil, M. C.: "Three-Dimensional Wake Flow Simulation for a 70-deg Blunted Cone During Reentry." Presented at the 19th International Symposium on Rarefied Gas Dynamics, Oxford, England, July 25-29, 1994.

[12]Bird, G. A.: Molecular Gas Dynamics and the Direct Simulation of Gas Flows, Clarendon Press, Oxford, 1994.

[13]Bird, G. A.: "Monte Carlo Simulation in Engineering Conte," Rarefied Gas Dynamics, Part I, edited by Sam S. Fisher, Vol. 74, Progress in Aeronautics and Astronautics, AIAA, pp. 239-255, New York, 1981.

[14]Anon: "Large Entry National Shock Tunnel (LENS) Description and Capabilities," Calspan-UB Research Center, February 1991.

[15]Holden, M.: "Recent Advances in Hypersonic Test Facilities and Experimental Research," AIAA Paper 93-5005, 30 Nov. - 3 Dec. 1993.

[16]Holden, M.: Personal Communication 1994, Calspan Corporation, Buffalo, New York.

[17]Borgnakke, C. and Larsen, P. S.: "Statistical Collision Model for Monte Carlo Simulation of Polyatomic Gas Mixture," Journal of Computational Physics, Vol. 18, No. 4, 1975, pp. 405-420.

[18]Hash, D. B.: Personal Communication, September 1994, North Carolina State University, Raleigh, North Carolina.

[19]Olynick, D. R. and Hassan, H. A.: "New Two-Temperature Dissociation Model for Reacting Flows," Journal of Thermophysics and Heat Transfer, Vol. 7, No. 4, Oct.-Dec. 1993, pp. 687-696.

[20]Olynick, D. R., Taylor, J. C., and Hassan, H. A.: "Comparisons Between DSMC and the Navier Stokes Equations for Reentry Flows," AIAA Paper 93-2810, July 1993.

Table 1. Tabulated Quantities Including Surface Data
(70-deg Blunted Cone with Sting).

FREESTREAM QUANTITIES

VELOCITY IN X-DIRECTION, M/S	=	3245.8
VELOCITY IN Y-DIRECTION, M/S	=	0.0
MACH NUMBER	=	15.64
SPEED OF SOUND, M/S	=	207.57
SPEED RATIO	=	13.08
MOST PROBABLE SPEED, M/S	=	248.10
TEMPERATURE, K	=	103.72
DENSITY, KG/M3	=	0.1306E-03
NUMBER DENSITY, M-3	=	0.2807E+22
PRESSURE, N/M2	=	0.4019E+01
GAMMAF	=	1.40
MOLECULAR WEIGHT	=	28.020
VISCOSITY, PA*S	=	0.7885E-05
REYNOLDS NUMBER	=	0.8193E+04
SHOCK REYNOLDS NUMBER	=	0.4364E+03
V-BAR PARAMETER (M/SQRT(REN))	=	0.173
CHI-BAR PARAMETER (M*3/SQRT(REN)	=	42.24
CHARACTERISTIC LENGTH, M	=	0.1524E+00
MEAN FREE PATH, M	=	0.3512E-03
KNUDSEN NUMBER	=	0.00230

GAS

SPECIES = N2
MOLE FRACTIONS = 1.0000
MOLECULAR WEIGHT = 28.0200
REFERENCE TEMPERATURE,K = 300.00 VISCOSITY-TEMPERATURE-EXPONENT= 0.75

WALL DATA:

TEMPERATURE K = 294.4 FRACTION SPECULAR REFLECTION= 0.0

REGION 1 FROM TIME 0.893E-03 TO TIME 0.122E-02 COLLISIONS:-
0.90769E+09
REGION 2 FROM TIME 0.446E-02 TO TIME 0.611E-02 COLLISIONS:-
0.91255E+09
REGION 3 FROM TIME 0.357E-02 TO TIME 0.489E-02 COLLISIONS:-
0.11210E+10
REGION 4 FROM TIME 0.178E-03 TO TIME 0.244E-03 COLLISIONS:-
0.63113E+07
REGION 5 FROM TIME 0.893E-03 TO TIME 0.122E-02 COLLISIONS:-
0.35900E+08
REGION 6 FROM TIME 0.268E-02 TO TIME 0.367E-02 COLLISIONS:-
0.20640E+09
REGION 7 FROM TIME 0.223E-03 TO TIME 0.306E-03 COLLISIONS:-
0.38379E+06
REGION 8 FROM TIME 0.178E-03 TO TIME 0.244E-03 COLLISIONS:-
0.14451E+06
REGION 9 FROM TIME 0.714E-03 TO TIME 0.977E-03 COLLISIONS:-
0.33005E+07
REGION 10 FROM TIME 0.223E-02 TO TIME 0.306E-02 COLLISIONS:-
0.86515E+08
REGION 11 FROM TIME 0.446E-02 TO TIME 0.611E-02 COLLISIONS:-
0.97600E+08
REGION 12 FROM TIME 0.446E-02 TO TIME 0.611E-02 COLLISIONS:-
0.27290E+08
REGION 13 FROM TIME 0.892E-02 TO TIME 0.122E-01 COLLISIONS:-
0.47230E+08
REGION 14 FROM TIME 0.134E-01 TO TIME 0.184E-01 COLLISIONS:-
0.32862E+09
REGION 15 FROM TIME 0.134E-01 TO TIME 0.184E-01 COLLISIONS:-
0.77555E+09

NUMBER OF MOVE SEGMENTS 0.48544E+11 RATIO 0.10017E+01
TOTAL NUMBER OF ENTERING MOLECULES = 1.67772E+07
0. EXCESS MOLECULE ERRORS 2668. REMOVAL ERRORS

TOTAL NUMBER OF SAMPLES 4400

489146 MOLECULES

SURFACE PROPERTIES

ELEMENT	X COORD m	Y COORD m	PRESSURE N/m*2	SHEAR ST. N/m*2	INC ENG W/m*2	REF ENG W/m*2	NET ENG W/m*2	SAMPLE SPECIES 1-
1	0.5158E-05	0.4434E-03	0.1221E+04	0.2304E+01	0.6814E+06	-0.3594E+06	0.3220E+06	0.2673E+06
2	0.2674E-04	0.1350E-02	0.1251E+04	0.5323E+01	0.6899E+06	-0.3693E+06	0.3206E+06	0.5727E+06
3	0.7230E-04	0.2296E-02	0.1266E+04	0.7274E+01	0.6889E+06	-0.3790E+06	0.3099E+06	0.4877E+06
4	0.1448E-03	0.3280E-02	0.1269E+04	0.7913E+01	0.6834E+06	-0.3799E+06	0.3036E+06	0.4393E+06
5	0.2474E-03	0.4303E-02	0.1261E+04	0.7873E+01	0.6785E+06	-0.3794E+06	0.2991E+06	0.4054E+06
6	0.3831E-03	0.5362E-02	0.1273E+04	0.1125E+02	0.6765E+06	-0.3830E+06	0.2935E+06	0.3895E+06
7	0.5553E-03	0.6456E-02	0.1267E+04	0.1342E+02	0.6651E+06	-0.3830E+06	0.2821E+06	0.3738E+06
8	0.7672E-03	0.7585E-02	0.1259E+04	0.1245E+02	0.6588E+06	-0.3817E+06	0.2771E+06	0.3593E+06
9	0.1022E-02	0.8746E-02	0.1259E+04	0.1423E+02	0.6535E+06	-0.3822E+06	0.2713E+06	0.3520E+06
10	0.1324E-02	0.9937E-02	0.1246E+04	0.1484E+02	0.6424E+06	-0.3801E+06	0.2623E+06	0.3414E+06
11	0.1676E-02	0.1116E-01	0.1240E+04	0.1383E+02	0.6335E+06	-0.3778E+06	0.2558E+06	0.3357E+06
12	0.2081E-02	0.1240E-01	0.1231E+04	0.1462E+02	0.6238E+06	-0.3769E+06	0.2469E+06	0.3293E+06
13	0.2530E-02	0.1367E-01	0.1227E+04	0.1484E+02	0.6149E+06	-0.3779E+06	0.2370E+06	0.3243E+06
14	0.2998E-02	0.1496E-01	0.1222E+04	0.1422E+02	0.6080E+06	-0.3787E+06	0.2293E+06	0.3165E+06
15	0.3472E-02	0.1626E-01	0.1237E+04	0.1412E+02	0.6082E+06	-0.3854E+06	0.2228E+06	0.3148E+06
16	0.3953E-02	0.1758E-01	0.1234E+04	0.1590E+02	0.6032E+06	-0.3861E+06	0.2171E+06	0.3086E+06
17	0.4440E-02	0.1892E-01	0.1212E+04	0.1493E+02	0.5903E+06	-0.3799E+06	0.2105E+06	0.2979E+06
18	0.4933E-02	0.2027E-01	0.1222E+04	0.1528E+02	0.5909E+06	-0.3842E+06	0.2067E+06	0.2968E+06
19	0.5432E-02	0.2164E-01	0.1213E+04	0.1625E+02	0.5844E+06	-0.3816E+06	0.2028E+06	0.2906E+06
20	0.5938E-02	0.2303E-01	0.1221E+04	0.1594E+02	0.5847E+06	-0.3849E+06	0.1998E+06	0.2895E+06
21	0.6450E-02	0.2444E-01	0.1209E+04	0.1542E+02	0.5779E+06	-0.3797E+06	0.1982E+06	0.2828E+06
22	0.6968E-02	0.2586E-01	0.1204E+04	0.1615E+02	0.5732E+06	-0.3782E+06	0.1950E+06	0.2789E+06
23	0.7492E-02	0.2730E-01	0.1207E+04	0.1608E+02	0.5735E+06	-0.3810E+06	0.1925E+06	0.2773E+06
24	0.8023E-02	0.2876E-01	0.1204E+04	0.1675E+02	0.5714E+06	-0.3818E+06	0.1897E+06	0.2742E+06
25	0.8560E-02	0.3024E-01	0.1200E+04	0.1649E+02	0.5688E+06	-0.3789E+06	0.1899E+06	0.2705E+06
26	0.9104E-02	0.3173E-01	0.1195E+04	0.1638E+02	0.5659E+06	-0.3773E+06	0.1886E+06	0.2674E+06
27	0.9653E-02	0.3324E-01	0.1193E+04	0.1749E+02	0.5632E+06	-0.3782E+06	0.1850E+06	0.2656E+06
28	0.1021E-01	0.3477E-01	0.1190E+04	0.1907E+02	0.5606E+06	-0.3770E+06	0.1836E+06	0.2626E+06
29	0.1077E-01	0.3631E-01	0.1181E+04	0.1827E+02	0.5555E+06	-0.3747E+06	0.1807E+06	0.2591E+06
30	0.1134E-01	0.3787E-01	0.1180E+04	0.1895E+02	0.5552E+06	-0.3731E+06	0.1821E+06	0.2569E+06
31	0.1191E-01	0.3945E-01	0.1174E+04	0.1756E+02	0.5512E+06	-0.3735E+06	0.1777E+06	0.2546E+06
32	0.1250E-01	0.4105E-01	0.1172E+04	0.2231E+02	0.5501E+06	-0.3724E+06	0.1778E+06	0.2526E+06
33	0.1308E-01	0.4266E-01	0.1168E+04	0.1853E+02	0.5460E+06	-0.3706E+06	0.1755E+06	0.2508E+06
34	0.1368E-01	0.4429E-01	0.1156E+04	0.2103E+02	0.5398E+06	-0.3677E+06	0.1722E+06	0.2471E+06
35	0.1428E-01	0.4594E-01	0.1164E+04	0.2052E+02	0.5432E+06	-0.3699E+06	0.1733E+06	0.2473E+06
36	0.1488E-01	0.4761E-01	0.1146E+04	0.2320E+02	0.5376E+06	-0.3643E+06	0.1733E+06	0.2426E+06
37	0.1550E-01	0.4929E-01	0.1149E+04	0.2109E+02	0.5363E+06	-0.3660E+06	0.1702E+06	0.2424E+06
38	0.1611E-01	0.5099E-01	0.1134E+04	0.2272E+02	0.5317E+06	-0.3611E+06	0.1706E+06	0.2379E+06
39	0.1674E-01	0.5271E-01	0.1133E+04	0.2284E+02	0.5314E+06	-0.3613E+06	0.1701E+06	0.2371E+06
40	0.1737E-01	0.5444E-01	0.1124E+04	0.2249E+02	0.5285E+06	-0.3579E+06	0.1706E+06	0.2344E+06
41	0.1801E-01	0.5619E-01	0.1117E+04	0.2421E+02	0.5248E+06	-0.3555E+06	0.1694E+06	0.2320E+06
42	0.1865E-01	0.5796E-01	0.1101E+04	0.2648E+02	0.5196E+06	-0.3498E+06	0.1698E+06	0.2271E+06
43	0.1930E-01	0.5975E-01	0.1094E+04	0.2592E+02	0.5172E+06	-0.3467E+06	0.1705E+06	0.2247E+06
44	0.1996E-01	0.6155E-01	0.1084E+04	0.2816E+02	0.5136E+06	-0.3428E+06	0.1708E+06	0.2219E+06
45	0.2062E-01	0.6337E-01	0.1067E+04	0.2911E+02	0.5097E+06	-0.3371E+06	0.1725E+06	0.2174E+06
46	0.2129E-01	0.6521E-01	0.1050E+04	0.3261E+02	0.5051E+06	-0.3306E+06	0.1745E+06	0.2125E+06
47	0.2196E-01	0.6707E-01	0.1022E+04	0.3622E+02	0.4943E+06	-0.3219E+06	0.1724E+06	0.2064E+06
48	0.2265E-01	0.6894E-01	0.9966E+03	0.3791E+02	0.4891E+06	-0.3122E+06	0.1768E+06	0.1998E+06
49	0.2333E-01	0.7083E-01	0.9662E+03	0.4455E+02	0.4816E+06	-0.3014E+06	0.1801E+06	0.1921E+06
50	0.2403E-01	0.7274E-01	0.9061E+03	0.5567E+02	0.4672E+06	-0.2789E+06	0.1883E+06	0.1774E+06
51	0.2441E-01	0.7379E-01	0.7247E+03	0.6696E+02	0.3939E+06	-0.2189E+06	0.1750E+06	0.1415E+05
52	0.2450E-01	0.7399E-01	0.6671E+03	0.7490E+02	0.3777E+06	-0.1997E+06	0.1780E+06	0.1366E+05
53	0.2460E-01	0.7419E-01	0.6044E+03	0.8298E+02	0.3486E+06	-0.1782E+06	0.1704E+06	0.1306E+05
54	0.2472E-01	0.7440E-01	0.5618E+03	0.8720E+02	0.3298E+06	-0.1655E+06	0.1643E+06	0.1280E+05
55	0.2487E-01	0.7462E-01	0.4911E+03	0.8138E+02	0.2946E+06	-0.1436E+06	0.1510E+06	0.1179E+05
56	0.2504E-01	0.7483E-01	0.4343E+03	0.8338E+02	0.2705E+06	-0.1266E+06	0.1438E+06	0.1094E+05
57	0.2523E-01	0.7505E-01	0.3835E+03	0.7855E+02	0.2407E+06	-0.1115E+06	0.1292E+06	0.1016E+05
58	0.2545E-01	0.7525E-01	0.3262E+03	0.7609E+02	0.2084E+06	-0.9453E+05	0.1139E+06	0.9039E+04
59	0.2570E-01	0.7545E-01	0.2754E+03	0.7044E+02	0.1776E+06	-0.7958E+05	0.9797E+05	0.7933E+04
60	0.2597E-01	0.7564E-01	0.2247E+03	0.6438E+02	0.1498E+06	-0.6478E+05	0.8503E+05	0.6721E+04
61	0.2628E-01	0.7580E-01	0.1876E+03	0.5729E+02	0.1283E+06	-0.5356E+05	0.7477E+05	0.5814E+04
62	0.2661E-01	0.7595E-01	0.1494E+03	0.5196E+02	0.1042E+06	-0.4298E+05	0.6120E+05	0.4848E+04
63	0.2697E-01	0.7606E-01	0.1195E+03	0.4390E+02	0.8604E+05	-0.3440E+05	0.5164E+05	0.4019E+04
64	0.2735E-01	0.7615E-01	0.9366E+02	0.3932E+02	0.7014E+05	-0.2717E+05	0.4297E+05	0.3310E+04
65	0.2775E-01	0.7619E-01	0.6994E+02	0.3316E+02	0.5384E+05	-0.2014E+05	0.3371E+05	0.2579E+04
66	0.2810E-01	0.7619E-01	0.5525E+02	0.2958E+02	0.4638E+05	-0.1617E+05	0.3022E+05	0.1367E+04
67	0.2839E-01	0.7617E-01	0.4386E+02	0.2489E+02	0.3636E+05	-0.1300E+05	0.2336E+05	0.1181E+04
68	0.2870E-01	0.7612E-01	0.3191E+02	0.1955E+02	0.2757E+05	-0.9438E+04	0.1813E+05	0.9710E+03
69	0.2904E-01	0.7604E-01	0.2656E+02	0.1736E+02	0.2313E+05	-0.8062E+04	0.1507E+05	0.8980E+03
70	0.2939E-01	0.7592E-01	0.1962E+02	0.1340E+02	0.1772E+05	-0.5964E+04	0.1175E+05	0.7000E+03
71	0.2975E-01	0.7575E-01	0.1337E+02	0.9795E+01	0.1299E+05	-0.4305E+04	0.8689E+04	0.5540E+03
72	0.3012E-01	0.7552E-01	0.8251E+01	0.6501E+01	0.8011E+04	-0.2675E+04	0.5335E+04	0.3690E+03
73	0.3047E-01	0.7524E-01	0.5405E+01	0.4680E+01	0.5543E+04	-0.1796E+04	0.3747E+04	0.2610E+03
74	0.3073E-01	0.7500E-01	0.4384E+01	0.3376E+01	0.4034E+04	-0.1433E+04	0.2601E+04	0.1090E+03
75	0.3091E-01	0.7479E-01	0.3602E+01	0.2537E+01	0.3715E+04	-0.1227E+04	0.2488E+04	0.1170E+03
76	0.3111E-01	0.7452E-01	0.2023E+01	0.1834E+01	0.2145E+04	-0.7265E+03	0.1418E+04	0.8900E+02
77	0.3132E-01	0.7418E-01	0.1922E+01	0.8647E+00	0.1538E+04	-0.6326E+03	0.9050E+03	0.9300E+02
78	0.3150E-01	0.7376E-01	0.1310E+01	0.7659E+00	0.1270E+04	-0.4727E+03	0.7970E+03	0.7400E+02
79	0.3165E-01	0.7327E-01	0.1575E+01	0.2295E+00	0.1190E+04	-0.5752E+03	0.6145E+03	0.9300E+02
80	0.3174E-01	0.7269E-01	0.2170E+01	-0.3617E+00	0.1456E+04	-0.6908E+03	0.7647E+03	0.1410E+03
81	0.3177E-01	0.7157E-01	0.2670E+01	-0.2679E+00	0.1717E+04	-0.8844E+03	0.8324E+03	0.4480E+03
82	0.3177E-01	0.6992E-01	0.3819E+01	-0.4750E+00	0.2252E+04	-0.1224E+04	0.1029E+04	0.6510E+03
83	0.3177E-01	0.6826E-01	0.5054E+01	-0.5577E+00	0.2726E+04	-0.1598E+04	0.1128E+04	0.8800E+03
84	0.3177E-01	0.6658E-01	0.5776E+01	-0.6743E+00	0.3086E+04	-0.1763E+04	0.1323E+04	0.9800E+03
85	0.3177E-01	0.6489E-01	0.6692E+01	-0.8698E+00	0.3488E+04	-0.2103E+04	0.1385E+04	0.1176E+04
86	0.3177E-01	0.6319E-01	0.7161E+01	-0.7010E+00	0.3654E+04	-0.2233E+04	0.1421E+04	0.1266E+04
87	0.3177E-01	0.6147E-01	0.7761E+01	-0.6108E+00	0.3849E+04	-0.2442E+04	0.1407E+04	0.1405E+04
88	0.3177E-01	0.5975E-01	0.8322E+01	-0.9050E+00	0.4100E+04	-0.2617E+04	0.1483E+04	0.1498E+04
89	0.3177E-01	0.5800E-01	0.8706E+01	-0.1070E+01	0.4266E+04	-0.2755E+04	0.1511E+04	0.1653E+04
90	0.3177E-01	0.5625E-01	0.9006E+01	-0.1072E+01	0.4444E+04	-0.2821E+04	0.1623E+04	0.1738E+04

91	0.3177E-01	0.5448E-01	0.9222E+01	-0.1075E+01	0.4440E+04	-0.2844E+04	0.1596E+04	0.1818E+04
92	0.3177E-01	0.5270E-01	0.9650E+01	-0.9588E+00	0.4665E+04	-0.3041E+04	0.1624E+04	0.1976E+04
93	0.3177E-01	0.5091E-01	0.1037E+02	-0.1183E+01	0.5020E+04	-0.3254E+04	0.1765E+04	0.2113E+04
94	0.3177E-01	0.4910E-01	0.1023E+02	-0.1019E+01	0.4991E+04	-0.3187E+04	0.1804E+04	0.2146E+04
95	0.3177E-01	0.4728E-01	0.1093E+02	-0.1195E+01	0.5110E+04	-0.3403E+04	0.1707E+04	0.2352E+04
96	0.3177E-01	0.4544E-01	0.1133E+02	-0.9597E+00	0.5441E+04	-0.3604E+04	0.1837E+04	0.2500E+04
97	0.3177E-01	0.4360E-01	0.1155E+02	-0.1122E+01	0.5548E+04	-0.3599E+04	0.1949E+04	0.2615E+04
98	0.3177E-01	0.4174E-01	0.1176E+02	-0.9965E+00	0.5464E+04	-0.3775E+04	0.1689E+04	0.2773E+04
99	0.3177E-01	0.3987E-01	0.1245E+02	-0.7540E+00	0.5934E+04	-0.3868E+04	0.2066E+04	0.2976E+04
100	0.3177E-01	0.3798E-01	0.1269E+02	-0.8041E+00	0.5872E+04	-0.4091E+04	0.1782E+04	0.3138E+04
101	0.3177E-01	0.3608E-01	0.1254E+02	-0.6503E+00	0.5822E+04	-0.3985E+04	0.1837E+04	0.3185E+04
102	0.3177E-01	0.3417E-01	0.1290E+02	-0.7126E+00	0.5831E+04	-0.4147E+04	0.1684E+04	0.3474E+04
103	0.3177E-01	0.3224E-01	0.1365E+02	-0.4062E+00	0.6179E+04	-0.4345E+04	0.1834E+04	0.3731E+04
104	0.3177E-01	0.3030E-01	0.1338E+02	-0.4576E+00	0.5967E+04	-0.4337E+04	0.1629E+04	0.3821E+04
105	0.3177E-01	0.2835E-01	0.1360E+02	-0.3247E+00	0.5890E+04	-0.4429E+04	0.1461E+04	0.4063E+04
106	0.3177E-01	0.2639E-01	0.1366E+02	0.7488E-01	0.5785E+04	-0.4502E+04	0.1283E+04	0.4211E+04
107	0.3197E-01	0.2429E-01	0.1340E+02	-0.9575E-01	0.5426E+04	-0.4460E+04	0.9658E+03	0.4995E+04
108	0.3279E-01	0.2215E-01	0.1307E+02	-0.8632E-01	0.5285E+04	-0.4376E+04	0.9094E+03	0.5434E+04
109	0.3445E-01	0.2038E-01	0.1330E+02	-0.2186E+00	0.5390E+04	-0.4507E+04	0.8832E+03	0.6075E+04
110	0.3680E-01	0.1934E-01	0.1287E+02	-0.2457E+00	0.5371E+04	-0.4346E+04	0.1025E+04	0.6295E+04
111	0.3833E-01	0.1905E-01	0.1329E+02	-0.4071E+00	0.5607E+04	-0.4507E+04	0.1100E+04	0.9770E+03
112	0.3876E-01	0.1905E-01	0.1306E+02	-0.2802E+00	0.5635E+04	-0.4315E+04	0.1319E+04	0.9940E+03
113	0.3921E-01	0.1905E-01	0.1185E+02	0.5808E-01	0.5163E+04	-0.4050E+04	0.1113E+04	0.9820E+03
114	0.3969E-01	0.1905E-01	0.1288E+02	-0.5892E+00	0.5607E+04	-0.4243E+04	0.1364E+04	0.1107E+04
115	0.4020E-01	0.1905E-01	0.1195E+02	-0.2558E+00	0.5518E+04	-0.3898E+04	0.1619E+04	0.1065E+04
116	0.4073E-01	0.1905E-01	0.1284E+02	-0.1977E+00	0.5630E+04	-0.4246E+04	0.1384E+04	0.1190E+04
117	0.4129E-01	0.1905E-01	0.1292E+02	-0.3188E+00	0.5867E+04	-0.4242E+04	0.1625E+04	0.1261E+04
118	0.4188E-01	0.1905E-01	0.1228E+02	-0.5488E+00	0.5554E+04	-0.3995E+04	0.1559E+04	0.1236E+04
119	0.4249E-01	0.1905E-01	0.1245E+02	-0.6323E+00	0.5839E+04	-0.3950E+04	0.1889E+04	0.1306E+04
120	0.4312E-01	0.1905E-01	0.1206E+02	-0.8320E+00	0.5704E+04	-0.3886E+04	0.1818E+04	0.1297E+04
121	0.4379E-01	0.1905E-01	0.1200E+02	-0.7894E+00	0.5738E+04	-0.3861E+04	0.1877E+04	0.1333E+04
122	0.4447E-01	0.1905E-01	0.1241E+02	-0.6671E+00	0.6160E+04	-0.3958E+04	0.2203E+04	0.1426E+04
123	0.4519E-01	0.1905E-01	0.1176E+02	-0.9732E+00	0.5902E+04	-0.3757E+04	0.2145E+04	0.1394E+04
124	0.4592E-01	0.1905E-01	0.1214E+02	-0.9399E+00	0.6210E+04	-0.3841E+04	0.2369E+04	0.1475E+04
125	0.4866E-01	0.1905E-01	0.1202E+02	-0.8729E+00	0.6059E+04	-0.3770E+04	0.2289E+04	0.9702E+04
126	0.5339E-01	0.1905E-01	0.1192E+02	-0.1210E+01	0.6278E+04	-0.3664E+04	0.2614E+04	0.9623E+04
127	0.5817E-01	0.1905E-01	0.1263E+02	-0.1514E+01	0.6865E+04	-0.3876E+04	0.2989E+04	0.1012E+05
128	0.6299E-01	0.1905E-01	0.1364E+02	-0.1777E+01	0.7522E+04	-0.4125E+04	0.3397E+04	0.1086E+05
129	0.6784E-01	0.1905E-01	0.1484E+02	-0.1796E+01	0.8422E+04	-0.4394E+04	0.4028E+04	0.1186E+05
130	0.7274E-01	0.1905E-01	0.1609E+02	-0.1898E+01	0.9211E+04	-0.4772E+04	0.4439E+04	0.1282E+05
131	0.7767E-01	0.1905E-01	0.1830E+02	-0.1979E+01	0.1045E+05	-0.5438E+04	0.5015E+04	0.1468E+05
132	0.8265E-01	0.1905E-01	0.1988E+02	-0.1856E+01	0.1141E+05	-0.5901E+04	0.5513E+04	0.1605E+05
133	0.8766E-01	0.1905E-01	0.2207E+02	-0.1667E+01	0.1264E+05	-0.6506E+04	0.6129E+04	0.1787E+05
134	0.9272E-01	0.1905E-01	0.2411E+02	-0.1497E+01	0.1364E+05	-0.7147E+04	0.6492E+04	0.1976E+05
135	0.9782E-01	0.1905E-01	0.2622E+02	-0.1443E+01	0.1501E+05	-0.7727E+04	0.7279E+04	0.2163E+05
136	0.1030E+00	0.1905E-01	0.2825E+02	-0.1158E+01	0.1612E+05	-0.8286E+04	0.7833E+04	0.2345E+05
137	0.1081E+00	0.1905E-01	0.3057E+02	-0.1070E+01	0.1734E+05	-0.9038E+04	0.8306E+04	0.2549E+05
138	0.1133E+00	0.1905E-01	0.3260E+02	-0.4195E+00	0.1869E+05	-0.9604E+04	0.9083E+04	0.2755E+05
139	0.1186E+00	0.1905E-01	0.3488E+02	-0.3140E+00	0.1978E+05	-0.1030E+05	0.9477E+04	0.2985E+05
140	0.1239E+00	0.1905E-01	0.3647E+02	0.7497E-01	0.2084E+05	-0.1086E+05	0.9979E+04	0.3145E+05
141	0.1292E+00	0.1905E-01	0.3828E+02	0.2274E+00	0.2171E+05	-0.1131E+05	0.1040E+05	0.3316E+05
142	0.1346E+00	0.1905E-01	0.3987E+02	0.5083E+00	0.2253E+05	-0.1175E+05	0.1078E+05	0.3483E+05
143	0.1400E+00	0.1905E-01	0.4201E+02	0.1010E+01	0.2379E+05	-0.1248E+05	0.1131E+05	0.3706E+05
144	0.1455E+00	0.1905E-01	0.4367E+02	0.1306E+01	0.2460E+05	-0.1297E+05	0.1163E+05	0.3882E+05
145	0.1510E+00	0.1905E-01	0.4469E+02	0.1808E+01	0.2540E+05	-0.1326E+05	0.1214E+05	0.3998E+05
146	0.1565E+00	0.1905E-01	0.4567E+02	0.1718E+01	0.2581E+05	-0.1361E+05	0.1220E+05	0.4123E+05
147	0.1621E+00	0.1905E-01	0.4660E+02	0.2328E+01	0.2620E+05	-0.1383E+05	0.1236E+05	0.4224E+05
148	0.1677E+00	0.1905E-01	0.4716E+02	0.2483E+01	0.2627E+05	-0.1410E+05	0.1217E+05	0.4331E+05
149	0.1734E+00	0.1905E-01	0.4890E+02	0.2794E+01	0.2751E+05	-0.1456E+05	0.1295E+05	0.4512E+05
150	0.1790E+00	0.1905E-01	0.4881E+02	0.2887E+01	0.2742E+05	-0.1453E+05	0.1290E+05	0.4535E+05
151	0.1848E+00	0.1905E-01	0.4897E+02	0.3344E+01	0.2749E+05	-0.1458E+05	0.1291E+05	0.4590E+05
152	0.1906E+00	0.1905E-01	0.4975E+02	0.3454E+01	0.2774E+05	-0.1485E+05	0.1290E+05	0.4698E+05
153	0.1964E+00	0.1905E-01	0.4982E+02	0.3728E+01	0.2766E+05	-0.1486E+05	0.1280E+05	0.4735E+05
154	0.2022E+00	0.1905E-01	0.4979E+02	0.3818E+01	0.2770E+05	-0.1486E+05	0.1284E+05	0.4769E+05
155	0.2081E+00	0.1905E-01	0.5027E+02	0.4015E+01	0.2826E+05	-0.1500E+05	0.1326E+05	0.4856E+05
156	0.2141E+00	0.1905E-01	0.5048E+02	0.4384E+01	0.2846E+05	-0.1505E+05	0.1340E+05	0.4892E+05
157	0.2200E+00	0.1905E-01	0.4968E+02	0.4537E+01	0.2798E+05	-0.1476E+05	0.1322E+05	0.4828E+05
158	0.2260E+00	0.1905E-01	0.4974E+02	0.4271E+01	0.2791E+05	-0.1484E+05	0.1307E+05	0.4879E+05
159	0.2321E+00	0.1905E-01	0.4936E+02	0.4507E+01	0.2801E+05	-0.1469E+05	0.1332E+05	0.4863E+05
160	0.2382E+00	0.1905E-01	0.4921E+02	0.4754E+01	0.2745E+05	-0.1468E+05	0.1277E+05	0.4903E+05
161	0.2443E+00	0.1905E-01	0.4920E+02	0.4894E+01	0.2749E+05	-0.1469E+05	0.1279E+05	0.4956E+05
162	0.2505E+00	0.1905E-01	0.4854E+02	0.5037E+01	0.2708E+05	-0.1447E+05	0.1261E+05	0.4901E+05
163	0.2567E+00	0.1905E-01	0.4768E+02	0.4934E+01	0.2669E+05	-0.1424E+05	0.1245E+05	0.4862E+05
164	0.2630E+00	0.1905E-01	0.4788E+02	0.5010E+01	0.2678E+05	-0.1427E+05	0.1250E+05	0.4902E+05
165	0.2693E+00	0.1905E-01	0.4619E+02	0.5133E+01	0.2598E+05	-0.1376E+05	0.1222E+05	0.4744E+05
166	0.2756E+00	0.1905E-01	0.4643E+02	0.5003E+01	0.2597E+05	-0.1388E+05	0.1210E+05	0.4824E+05
167	0.2820E+00	0.1905E-01	0.4477E+02	0.5104E+01	0.2536E+05	-0.1334E+05	0.1202E+05	0.4658E+05
168	0.2884E+00	0.1905E-01	0.4454E+02	0.5287E+01	0.2527E+05	-0.1324E+05	0.1204E+05	0.4665E+05
169	0.2948E+00	0.1905E-01	0.4436E+02	0.5194E+01	0.2519E+05	-0.1318E+05	0.1201E+05	0.4660E+05
170	0.3013E+00	0.1905E-01	0.4381E+02	0.5288E+01	0.2495E+05	-0.1299E+05	0.1196E+05	0.4653E+05
171	0.3079E+00	0.1905E-01	0.4342E+02	0.5485E+01	0.2489E+05	-0.1286E+05	0.1203E+05	0.4607E+05
172	0.3145E+00	0.1905E-01	0.4266E+02	0.5425E+01	0.2455E+05	-0.1270E+05	0.1185E+05	0.4557E+05
173	0.3211E+00	0.1905E-01	0.4186E+02	0.5373E+01	0.2414E+05	-0.1240E+05	0.1175E+05	0.4510E+05
174	0.3277E+00	0.1905E-01	0.4158E+02	0.5305E+01	0.2384E+05	-0.1231E+05	0.1152E+05	0.4483E+05
175	0.3344E+00	0.1905E-01	0.4123E+02	0.5449E+01	0.2375E+05	-0.1223E+05	0.1152E+05	0.4476E+05
176	0.3411E+00	0.1905E-01	0.4017E+02	0.5282E+01	0.2311E+05	-0.1189E+05	0.1122E+05	0.4396E+05
177	0.3479E+00	0.1905E-01	0.4032E+02	0.5596E+01	0.2327E+05	-0.1197E+05	0.1131E+05	0.4443E+05
178	0.3547E+00	0.1905E-01	0.3903E+02	0.5426E+01	0.2257E+05	-0.1154E+05	0.1103E+05	0.4298E+05
179	0.3616E+00	0.1905E-01	0.3827E+02	0.5435E+01	0.2220E+05	-0.1132E+05	0.1088E+05	0.4237E+05
180	0.3685E+00	0.1905E-01	0.3736E+02	0.5312E+01	0.2188E+05	-0.1099E+05	0.1088E+05	0.4153E+05
181	0.3754E+00	0.1905E-01	0.3741E+02	0.5593E+01	0.2201E+05	-0.1099E+05	0.1102E+05	0.4168E+05
182	0.3824E+00	0.1905E-01	0.3568E+02	0.5796E+01	0.2133E+05	-0.1047E+05	0.1086E+05	0.4001E+05
183	0.3894E+00	0.1905E-01	0.3399E+02	0.6177E+01	0.2063E+05	-0.9921E+04	0.1071E+05	0.3810E+05

184 0.3965E+00 0.1905E-01 0.3042E+02 0.7399E+01 0.1954E+05-0.8737E+04 0.1080E+05 0.3360E+05

NONDIMENSIONAL SURFACE QUANTITIES
0.5*ROF*UF**2= 0.6879E+03 0.5*ROF*UF**3= 0.2233E+07

ELEMENT	X, m	Y, m	S/Rn	CP	CF	CH
1	0.516E-05	0.443E-03	0.116E-01	0.177E+01	0.335E-02	0.144E+00
2	0.267E-04	0.135E-02	0.354E-01	0.182E+01	0.774E-02	0.144E+00
3	0.723E-04	0.230E-02	0.603E-01	0.184E+01	0.106E-01	0.139E+00
4	0.145E-03	0.328E-02	0.862E-01	0.185E+01	0.115E-01	0.136E+00
5	0.247E-03	0.430E-02	0.113E+00	0.183E+01	0.114E-01	0.134E+00
6	0.383E-03	0.536E-02	0.141E+00	0.185E+01	0.164E-01	0.131E+00
7	0.555E-03	0.646E-02	0.170E+00	0.184E+01	0.195E-01	0.126E+00
8	0.767E-03	0.759E-02	0.200E+00	0.183E+01	0.181E-01	0.124E+00
9	0.102E-02	0.875E-02	0.232E+00	0.183E+01	0.207E-01	0.122E+00
10	0.132E-02	0.994E-02	0.264E+00	0.181E+01	0.216E-01	0.117E+00
11	0.168E-02	0.112E-01	0.297E+00	0.180E+01	0.201E-01	0.115E+00
12	0.208E-02	0.124E-01	0.332E+00	0.179E+01	0.213E-01	0.111E+00
13	0.253E-02	0.137E-01	0.367E+00	0.178E+01	0.216E-01	0.106E+00
14	0.300E-02	0.150E-01	0.403E+00	0.178E+01	0.207E-01	0.103E+00
15	0.347E-02	0.163E-01	0.439E+00	0.180E+01	0.205E-01	0.998E-01
16	0.395E-02	0.176E-01	0.476E+00	0.179E+01	0.231E-01	0.972E-01
17	0.444E-02	0.189E-01	0.513E+00	0.176E+01	0.217E-01	0.943E-01
18	0.493E-02	0.203E-01	0.551E+00	0.178E+01	0.222E-01	0.926E-01
19	0.543E-02	0.216E-01	0.590E+00	0.176E+01	0.236E-01	0.908E-01
20	0.594E-02	0.230E-01	0.628E+00	0.178E+01	0.232E-01	0.895E-01
21	0.645E-02	0.244E-01	0.668E+00	0.176E+01	0.224E-01	0.888E-01
22	0.697E-02	0.259E-01	0.707E+00	0.175E+01	0.235E-01	0.873E-01
23	0.749E-02	0.273E-01	0.748E+00	0.175E+01	0.234E-01	0.862E-01
24	0.802E-02	0.288E-01	0.788E+00	0.175E+01	0.244E-01	0.850E-01
25	0.856E-02	0.302E-01	0.830E+00	0.174E+01	0.240E-01	0.850E-01
26	0.910E-02	0.317E-01	0.871E+00	0.174E+01	0.238E-01	0.845E-01
27	0.965E-02	0.332E-01	0.913E+00	0.173E+01	0.254E-01	0.829E-01
28	0.102E-01	0.348E-01	0.956E+00	0.173E+01	0.277E-01	0.822E-01
29	0.108E-01	0.363E-01	0.999E+00	0.172E+01	0.266E-01	0.809E-01
30	0.113E-01	0.379E-01	0.104E+01	0.172E+01	0.275E-01	0.816E-01
31	0.119E-01	0.395E-01	0.109E+01	0.171E+01	0.255E-01	0.796E-01
32	0.125E-01	0.410E-01	0.113E+01	0.170E+01	0.324E-01	0.796E-01
33	0.131E-01	0.427E-01	0.118E+01	0.170E+01	0.269E-01	0.786E-01
34	0.137E-01	0.443E-01	0.122E+01	0.168E+01	0.306E-01	0.771E-01
35	0.143E-01	0.459E-01	0.127E+01	0.169E+01	0.298E-01	0.776E-01
36	0.149E-01	0.476E-01	0.131E+01	0.167E+01	0.337E-01	0.776E-01
37	0.155E-01	0.493E-01	0.136E+01	0.167E+01	0.307E-01	0.762E-01
38	0.161E-01	0.510E-01	0.141E+01	0.165E+01	0.330E-01	0.764E-01
39	0.167E-01	0.527E-01	0.146E+01	0.165E+01	0.332E-01	0.762E-01
40	0.174E-01	0.544E-01	0.151E+01	0.163E+01	0.327E-01	0.764E-01
41	0.180E-01	0.562E-01	0.155E+01	0.162E+01	0.352E-01	0.758E-01
42	0.187E-01	0.580E-01	0.160E+01	0.160E+01	0.385E-01	0.761E-01
43	0.193E-01	0.597E-01	0.165E+01	0.159E+01	0.377E-01	0.763E-01
44	0.200E-01	0.616E-01	0.170E+01	0.158E+01	0.409E-01	0.765E-01
45	0.206E-01	0.634E-01	0.176E+01	0.155E+01	0.423E-01	0.773E-01
46	0.213E-01	0.652E-01	0.181E+01	0.153E+01	0.474E-01	0.781E-01
47	0.220E-01	0.671E-01	0.186E+01	0.149E+01	0.527E-01	0.772E-01
48	0.226E-01	0.689E-01	0.191E+01	0.145E+01	0.551E-01	0.792E-01
49	0.233E-01	0.708E-01	0.196E+01	0.140E+01	0.648E-01	0.807E-01
50	0.240E-01	0.727E-01	0.202E+01	0.132E+01	0.809E-01	0.843E-01
51	0.244E-01	0.738E-01	0.205E+01	0.105E+01	0.973E-01	0.784E-01
52	0.245E-01	0.740E-01	0.205E+01	0.970E+00	0.109E+00	0.797E-01
53	0.246E-01	0.742E-01	0.206E+01	0.879E+00	0.121E+00	0.763E-01
54	0.247E-01	0.744E-01	0.206E+01	0.817E+00	0.127E+00	0.736E-01
55	0.249E-01	0.746E-01	0.207E+01	0.714E+00	0.118E+00	0.676E-01
56	0.250E-01	0.748E-01	0.208E+01	0.631E+00	0.121E+00	0.644E-01
57	0.252E-01	0.750E-01	0.209E+01	0.558E+00	0.114E+00	0.578E-01
58	0.254E-01	0.753E-01	0.209E+01	0.474E+00	0.111E+00	0.510E-01
59	0.257E-01	0.755E-01	0.210E+01	0.400E+00	0.102E+00	0.439E-01
60	0.260E-01	0.756E-01	0.211E+01	0.327E+00	0.936E-01	0.381E-01
61	0.263E-01	0.758E-01	0.212E+01	0.273E+00	0.833E-01	0.335E-01
62	0.266E-01	0.759E-01	0.213E+01	0.217E+00	0.755E-01	0.274E-01
63	0.270E-01	0.761E-01	0.214E+01	0.174E+00	0.638E-01	0.231E-01
64	0.273E-01	0.761E-01	0.215E+01	0.136E+00	0.572E-01	0.192E-01
65	0.278E-01	0.762E-01	0.216E+01	0.102E+00	0.482E-01	0.151E-01
66	0.281E-01	0.762E-01	0.217E+01	0.803E-01	0.430E-01	0.135E-01
67	0.284E-01	0.762E-01	0.218E+01	0.638E-01	0.362E-01	0.105E-01
68	0.287E-01	0.761E-01	0.219E+01	0.464E-01	0.284E-01	0.812E-02
69	0.290E-01	0.760E-01	0.219E+01	0.386E-01	0.252E-01	0.675E-02
70	0.294E-01	0.759E-01	0.220E+01	0.285E-01	0.195E-01	0.526E-02
71	0.298E-01	0.757E-01	0.221E+01	0.194E-01	0.142E-01	0.389E-02
72	0.301E-01	0.755E-01	0.223E+01	0.120E-01	0.945E-02	0.239E-02
73	0.305E-01	0.752E-01	0.224E+01	0.786E-02	0.680E-02	0.168E-02
74	0.307E-01	0.750E-01	0.225E+01	0.637E-02	0.491E-02	0.116E-02
75	0.309E-01	0.748E-01	0.225E+01	0.524E-02	0.369E-02	0.111E-02
76	0.311E-01	0.745E-01	0.226E+01	0.294E-02	0.267E-02	0.635E-03
77	0.313E-01	0.742E-01	0.227E+01	0.279E-02	0.126E-02	0.405E-03
78	0.315E-01	0.738E-01	0.229E+01	0.190E-02	0.111E-02	0.357E-03
79	0.317E-01	0.733E-01	0.230E+01	0.229E-02	0.334E-03	0.275E-03
80	0.317E-01	0.727E-01	0.231E+01	0.316E-02	-0.526E-03	0.342E-03
81	0.318E-01	0.716E-01	0.234E+01	0.388E-02	-0.389E-03	0.373E-03
82	0.318E-01	0.699E-01	0.239E+01	0.555E-02	-0.691E-03	0.461E-03
83	0.318E-01	0.683E-01	0.243E+01	0.735E-02	-0.811E-03	0.505E-03
84	0.318E-01	0.666E-01	0.247E+01	0.840E-02	-0.980E-03	0.592E-03
85	0.318E-01	0.649E-01	0.252E+01	0.973E-02	-0.126E-02	0.620E-03
86	0.318E-01	0.632E-01	0.256E+01	0.104E-01	-0.102E-02	0.636E-03
87	0.318E-01	0.615E-01	0.261E+01	0.113E-01	-0.888E-03	0.630E-03

88	0.318E-01	0.597E-01	0.265E+01	0.121E-01	-0.132E-02	0.664E-03
89	0.318E-01	0.580E-01	0.270E+01	0.127E-01	-0.156E-02	0.677E-03
90	0.318E-01	0.562E-01	0.275E+01	0.131E-01	-0.156E-02	0.727E-03
91	0.318E-01	0.545E-01	0.279E+01	0.134E-01	-0.156E-02	0.715E-03
92	0.318E-01	0.527E-01	0.284E+01	0.140E-01	-0.139E-02	0.727E-03
93	0.318E-01	0.509E-01	0.289E+01	0.151E-01	-0.172E-02	0.791E-03
94	0.318E-01	0.491E-01	0.293E+01	0.149E-01	-0.148E-02	0.808E-03
95	0.318E-01	0.473E-01	0.298E+01	0.159E-01	-0.174E-02	0.764E-03
96	0.318E-01	0.454E-01	0.303E+01	0.165E-01	-0.140E-02	0.823E-03
97	0.318E-01	0.436E-01	0.308E+01	0.168E-01	-0.163E-02	0.873E-03
98	0.318E-01	0.417E-01	0.313E+01	0.171E-01	-0.145E-02	0.756E-03
99	0.318E-01	0.399E-01	0.318E+01	0.181E-01	-0.110E-02	0.925E-03
100	0.318E-01	0.380E-01	0.323E+01	0.184E-01	-0.117E-02	0.798E-03
101	0.318E-01	0.361E-01	0.328E+01	0.182E-01	-0.945E-03	0.823E-03
102	0.318E-01	0.342E-01	0.333E+01	0.188E-01	-0.104E-02	0.754E-03
103	0.318E-01	0.322E-01	0.338E+01	0.198E-01	-0.590E-03	0.821E-03
104	0.318E-01	0.303E-01	0.343E+01	0.195E-01	-0.665E-03	0.730E-03
105	0.318E-01	0.284E-01	0.348E+01	0.198E-01	-0.472E-03	0.654E-03
106	0.318E-01	0.264E-01	0.353E+01	0.199E-01	0.109E-03	0.574E-03
107	0.320E-01	0.243E-01	0.358E+01	0.195E-01	-0.139E-03	0.433E-03
108	0.328E-01	0.222E-01	0.364E+01	0.190E-01	-0.125E-03	0.407E-03
109	0.344E-01	0.204E-01	0.371E+01	0.193E-01	-0.318E-03	0.396E-03
110	0.368E-01	0.193E-01	0.378E+01	0.187E-01	-0.357E-03	0.459E-03
111	0.383E-01	0.191E-01	0.382E+01	0.193E-01	-0.592E-03	0.493E-03
112	0.388E-01	0.191E-01	0.383E+01	0.190E-01	-0.407E-03	0.591E-03
113	0.392E-01	0.191E-01	0.384E+01	0.172E-01	0.844E-04	0.498E-03
114	0.397E-01	0.191E-01	0.385E+01	0.187E-01	-0.857E-03	0.611E-03
115	0.402E-01	0.191E-01	0.387E+01	0.174E-01	-0.372E-03	0.725E-03
116	0.407E-01	0.191E-01	0.388E+01	0.187E-01	-0.287E-03	0.620E-03
117	0.413E-01	0.191E-01	0.389E+01	0.188E-01	-0.463E-03	0.728E-03
118	0.419E-01	0.191E-01	0.391E+01	0.179E-01	-0.798E-03	0.698E-03
119	0.425E-01	0.191E-01	0.393E+01	0.181E-01	-0.919E-03	0.846E-03
120	0.431E-01	0.191E-01	0.394E+01	0.175E-01	-0.121E-02	0.814E-03
121	0.438E-01	0.191E-01	0.396E+01	0.174E-01	-0.115E-02	0.841E-03
122	0.445E-01	0.191E-01	0.398E+01	0.180E-01	-0.970E-03	0.986E-03
123	0.452E-01	0.191E-01	0.400E+01	0.171E-01	-0.141E-02	0.961E-03
124	0.459E-01	0.191E-01	0.402E+01	0.176E-01	-0.137E-02	0.106E-02
125	0.487E-01	0.191E-01	0.409E+01	0.175E-01	-0.127E-02	0.103E-02
126	0.534E-01	0.191E-01	0.421E+01	0.173E-01	-0.176E-02	0.117E-02
127	0.582E-01	0.191E-01	0.434E+01	0.184E-01	-0.220E-02	0.134E-02
128	0.630E-01	0.191E-01	0.446E+01	0.198E-01	-0.258E-02	0.152E-02
129	0.678E-01	0.191E-01	0.459E+01	0.216E-01	-0.261E-02	0.180E-02
130	0.727E-01	0.191E-01	0.472E+01	0.234E-01	-0.276E-02	0.199E-02
131	0.777E-01	0.191E-01	0.485E+01	0.266E-01	-0.288E-02	0.225E-02
132	0.826E-01	0.191E-01	0.498E+01	0.289E-01	-0.270E-02	0.247E-02
133	0.877E-01	0.191E-01	0.511E+01	0.321E-01	-0.242E-02	0.275E-02
134	0.927E-01	0.191E-01	0.524E+01	0.350E-01	-0.218E-02	0.291E-02
135	0.978E-01	0.191E-01	0.538E+01	0.381E-01	-0.210E-02	0.326E-02
136	0.103E+00	0.191E-01	0.551E+01	0.411E-01	-0.168E-02	0.351E-02
137	0.108E+00	0.191E-01	0.565E+01	0.444E-01	-0.156E-02	0.372E-02
138	0.113E+00	0.191E-01	0.579E+01	0.474E-01	-0.610E-03	0.407E-02
139	0.119E+00	0.191E-01	0.592E+01	0.507E-01	-0.456E-03	0.424E-02
140	0.124E+00	0.191E-01	0.606E+01	0.530E-01	0.109E-03	0.447E-02
141	0.129E+00	0.191E-01	0.620E+01	0.556E-01	0.331E-03	0.466E-02
142	0.135E+00	0.191E-01	0.634E+01	0.579E-01	0.739E-03	0.483E-02
143	0.140E+00	0.191E-01	0.649E+01	0.611E-01	0.147E-02	0.507E-02
144	0.145E+00	0.191E-01	0.663E+01	0.635E-01	0.190E-02	0.521E-02
145	0.151E+00	0.191E-01	0.677E+01	0.650E-01	0.263E-02	0.544E-02
146	0.157E+00	0.191E-01	0.692E+01	0.664E-01	0.250E-02	0.546E-02
147	0.162E+00	0.191E-01	0.707E+01	0.677E-01	0.338E-02	0.554E-02
148	0.168E+00	0.191E-01	0.721E+01	0.685E-01	0.361E-02	0.545E-02
149	0.173E+00	0.191E-01	0.736E+01	0.711E-01	0.406E-02	0.580E-02
150	0.179E+00	0.191E-01	0.751E+01	0.710E-01	0.420E-02	0.578E-02
151	0.185E+00	0.191E-01	0.766E+01	0.712E-01	0.486E-02	0.578E-02
152	0.191E+00	0.191E-01	0.781E+01	0.723E-01	0.502E-02	0.578E-02
153	0.196E+00	0.191E-01	0.797E+01	0.724E-01	0.542E-02	0.573E-02
154	0.202E+00	0.191E-01	0.812E+01	0.724E-01	0.555E-02	0.575E-02
155	0.208E+00	0.191E-01	0.827E+01	0.731E-01	0.584E-02	0.594E-02
156	0.214E+00	0.191E-01	0.843E+01	0.734E-01	0.637E-02	0.600E-02
157	0.220E+00	0.191E-01	0.859E+01	0.722E-01	0.660E-02	0.592E-02
158	0.226E+00	0.191E-01	0.874E+01	0.723E-01	0.621E-02	0.585E-02
159	0.232E+00	0.191E-01	0.890E+01	0.717E-01	0.655E-02	0.597E-02
160	0.238E+00	0.191E-01	0.906E+01	0.715E-01	0.691E-02	0.572E-02
161	0.244E+00	0.191E-01	0.922E+01	0.715E-01	0.711E-02	0.573E-02
162	0.251E+00	0.191E-01	0.939E+01	0.706E-01	0.732E-02	0.565E-02
163	0.257E+00	0.191E-01	0.955E+01	0.693E-01	0.717E-02	0.557E-02
164	0.263E+00	0.191E-01	0.971E+01	0.696E-01	0.728E-02	0.560E-02
165	0.269E+00	0.191E-01	0.988E+01	0.672E-01	0.746E-02	0.547E-02
166	0.276E+00	0.191E-01	0.100E+02	0.675E-01	0.727E-02	0.542E-02
167	0.282E+00	0.191E-01	0.102E+02	0.651E-01	0.742E-02	0.538E-02
168	0.288E+00	0.191E-01	0.104E+02	0.648E-01	0.769E-02	0.539E-02
169	0.295E+00	0.191E-01	0.105E+02	0.645E-01	0.755E-02	0.538E-02
170	0.301E+00	0.191E-01	0.107E+02	0.637E-01	0.769E-02	0.536E-02
171	0.308E+00	0.191E-01	0.109E+02	0.631E-01	0.797E-02	0.539E-02
172	0.314E+00	0.191E-01	0.111E+02	0.620E-01	0.789E-02	0.531E-02
173	0.321E+00	0.191E-01	0.112E+02	0.608E-01	0.781E-02	0.526E-02
174	0.328E+00	0.191E-01	0.114E+02	0.604E-01	0.771E-02	0.516E-02
175	0.334E+00	0.191E-01	0.116E+02	0.599E-01	0.792E-02	0.516E-02
176	0.341E+00	0.191E-01	0.118E+02	0.584E-01	0.768E-02	0.502E-02
177	0.348E+00	0.191E-01	0.119E+02	0.586E-01	0.813E-02	0.506E-02
178	0.355E+00	0.191E-01	0.121E+02	0.567E-01	0.789E-02	0.494E-02
179	0.362E+00	0.191E-01	0.123E+02	0.556E-01	0.790E-02	0.487E-02
180	0.368E+00	0.191E-01	0.125E+02	0.543E-01	0.772E-02	0.487E-02

181	0.375E+00	0.191E-01	0.127E+02	0.544E-01	0.813E-02	0.493E-02
182	0.382E+00	0.191E-01	0.128E+02	0.519E-01	0.843E-02	0.486E-02
183	0.389E+00	0.191E-01	0.130E+02	0.494E-01	0.898E-02	0.480E-02
184	0.396E+00	0.191E-01	0.132E+02	0.442E-01	0.108E-01	0.484E-02

20

PRESS-DRAG, N= 0.19354E+02 FRIC-DRAG, N= 0.41220E+00 DRAG, N= 0.19766E+02

CDP= 0.15423E+01 CDF= 0.32847E-01 CD= 0.15751E+01

70° BLUNTED CONE WITH STING

R_b = 7.62 cm, R_n/R_b = 0.50, R_c/R_b = 0.05, R_s/R_b = 0.25, L_s/R_b = 6

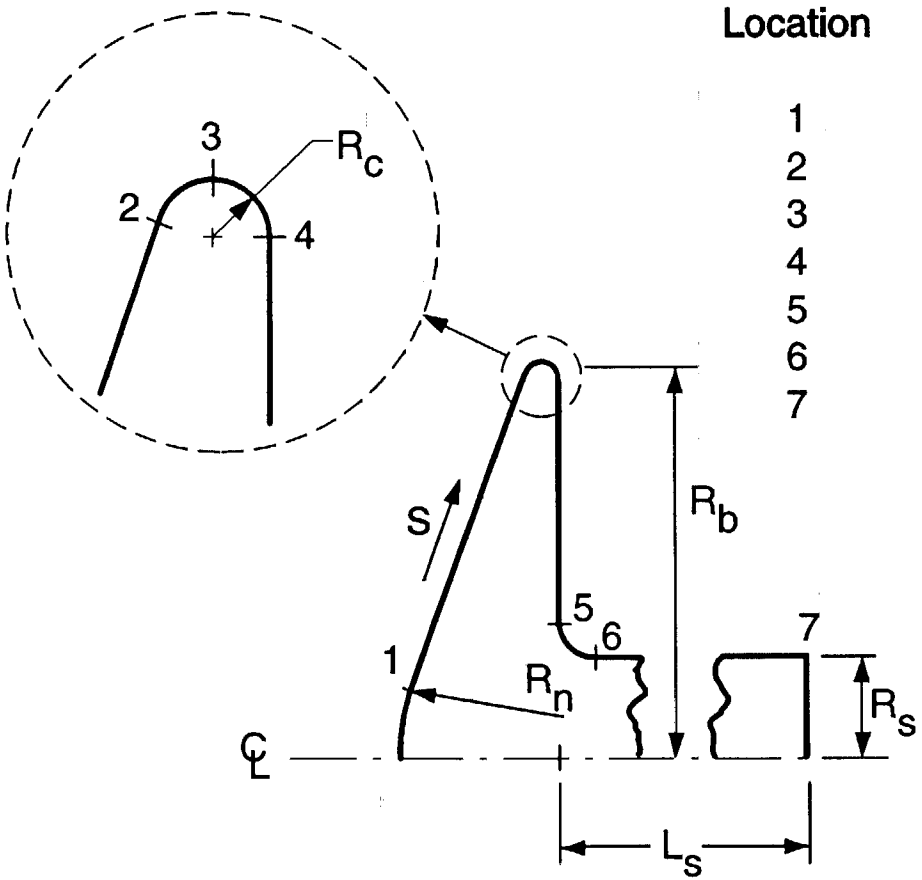

Location	s/R_n	X, cm	Y, cm
1	0.349	0.230	1.303
2	2.043	2.438	7.369
3	2.166	2.796	7.620
4	2.323	3.177	7.239
5	3.557	3.177	2.537
6	3.817	3.809	1.905
7	15.651	48.897	1.905

Fig. 1 Model configuration (base-sting fillet radius = 0.083 R_b).

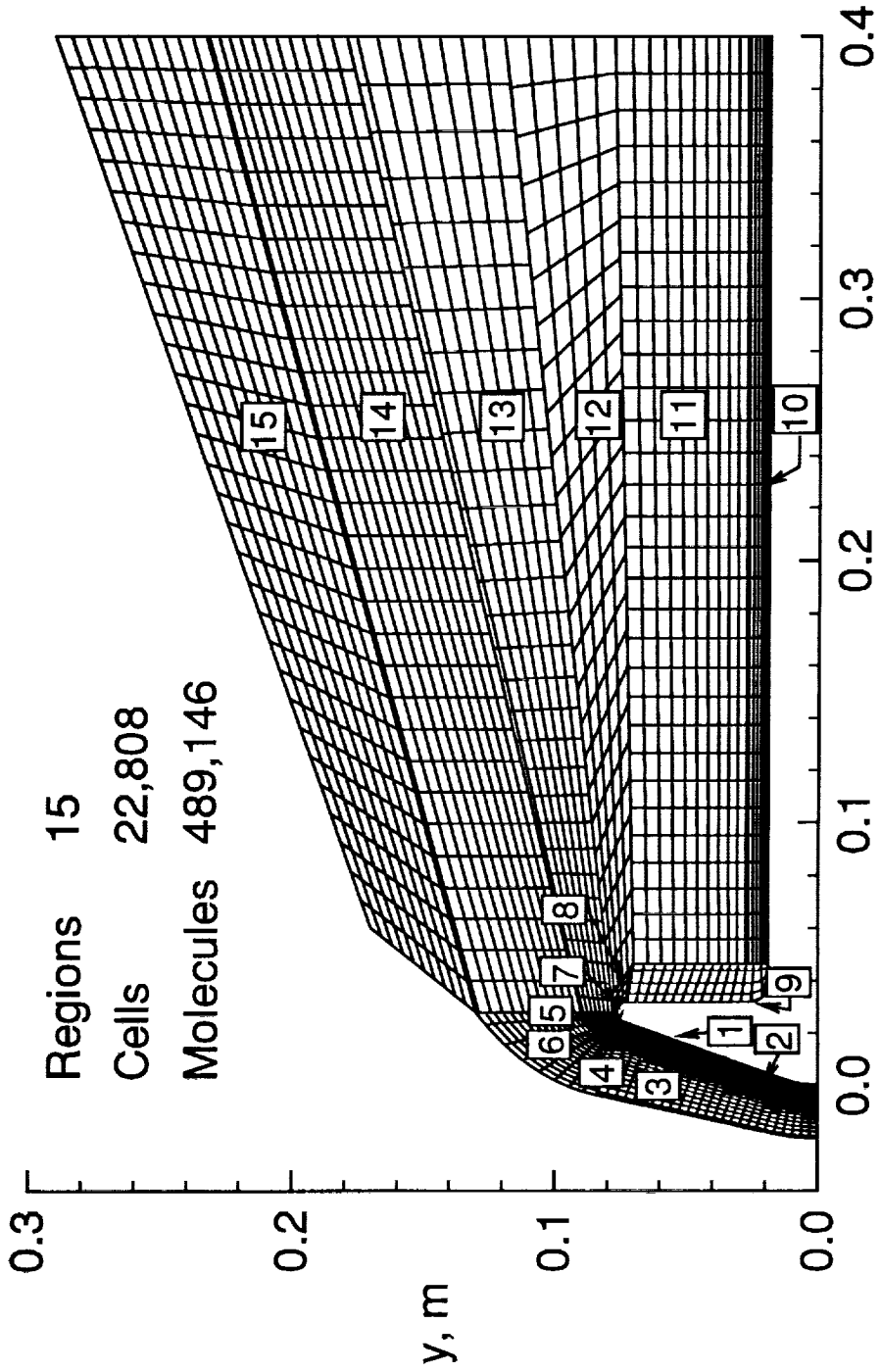

(a) Overall grid

Fig. 2 Computational domain and grid (reduced for clarity).

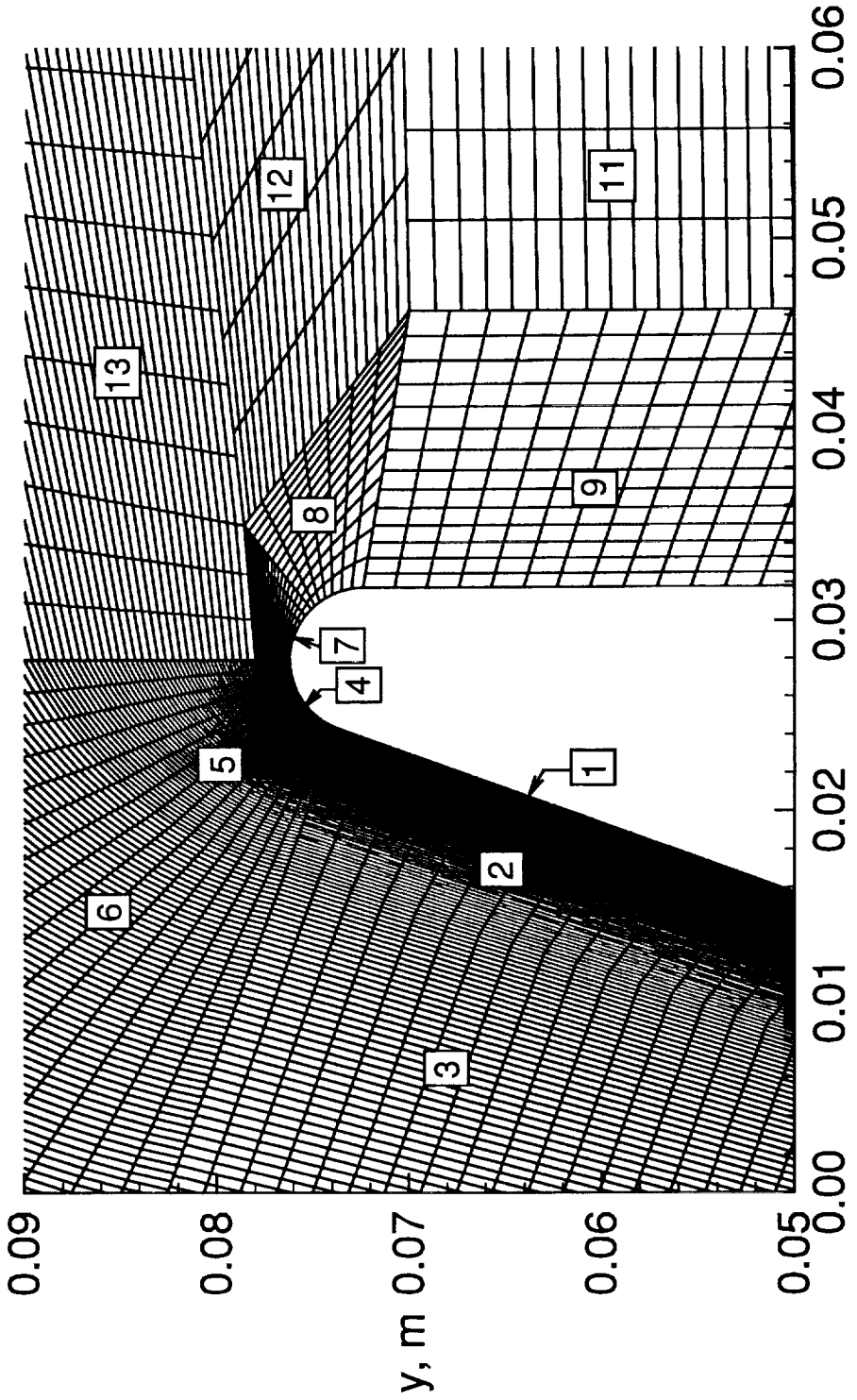

(b) Exploded view of grid for corner expansion

Fig. 2 Concluded.

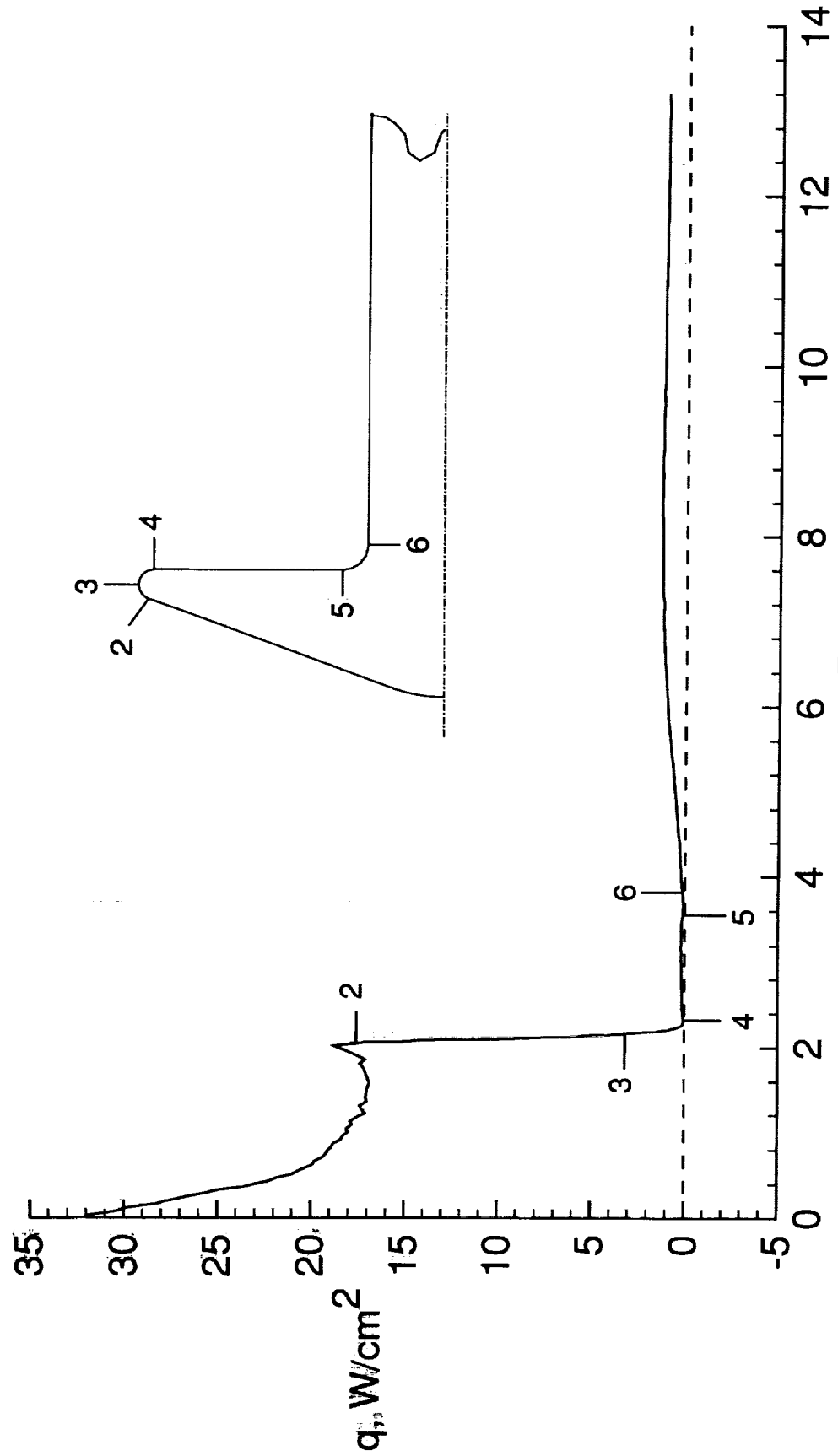

(a) Cartesian plot

Fig. 3 Surface heating rate distribution.

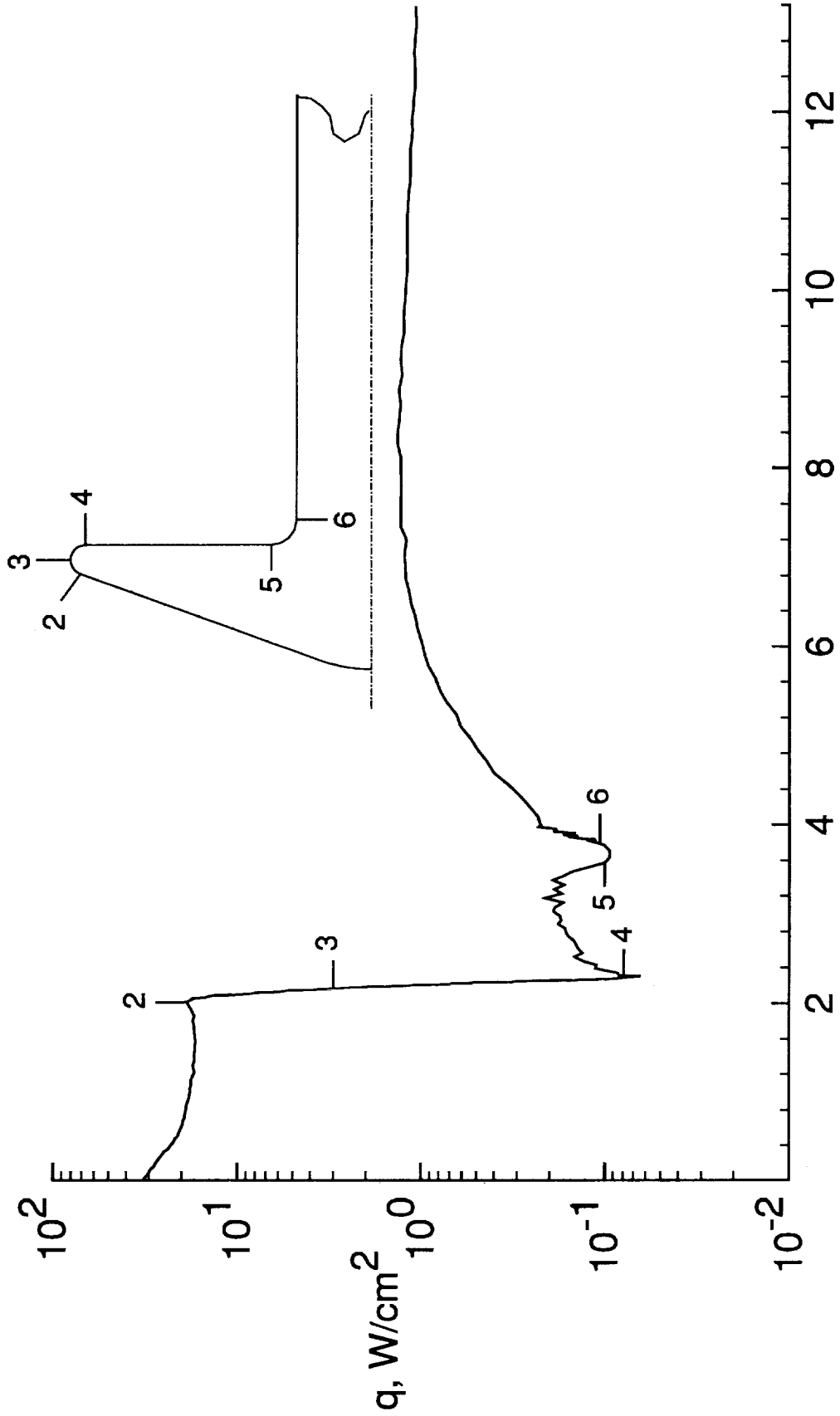

(b) Semilog plot

Fig. 3 Concluded.

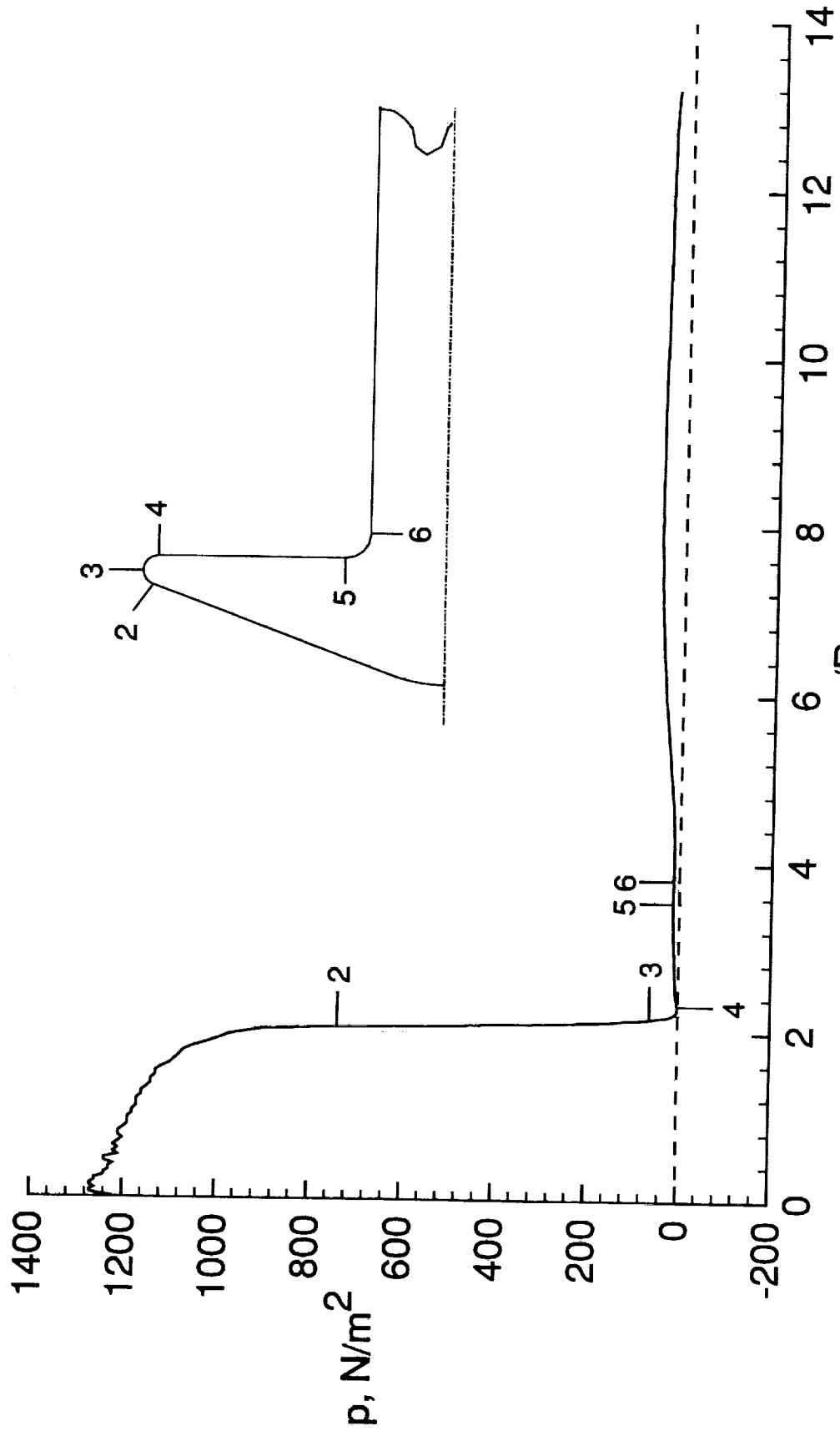

(a) Cartesian plot

Fig. 4 Surface pressure distribution.

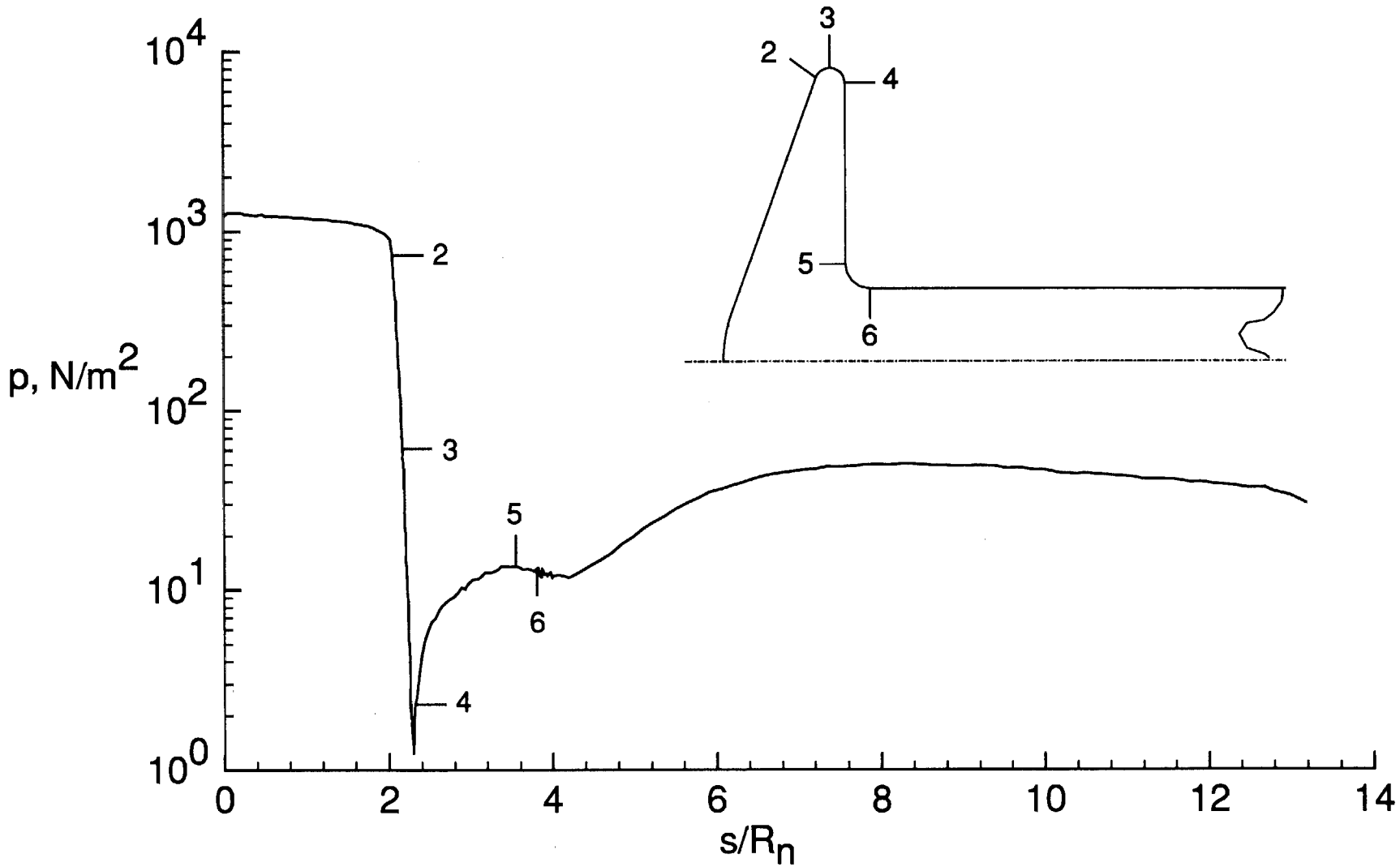

(b) Semilog plot

Fig. 4 Concluded.

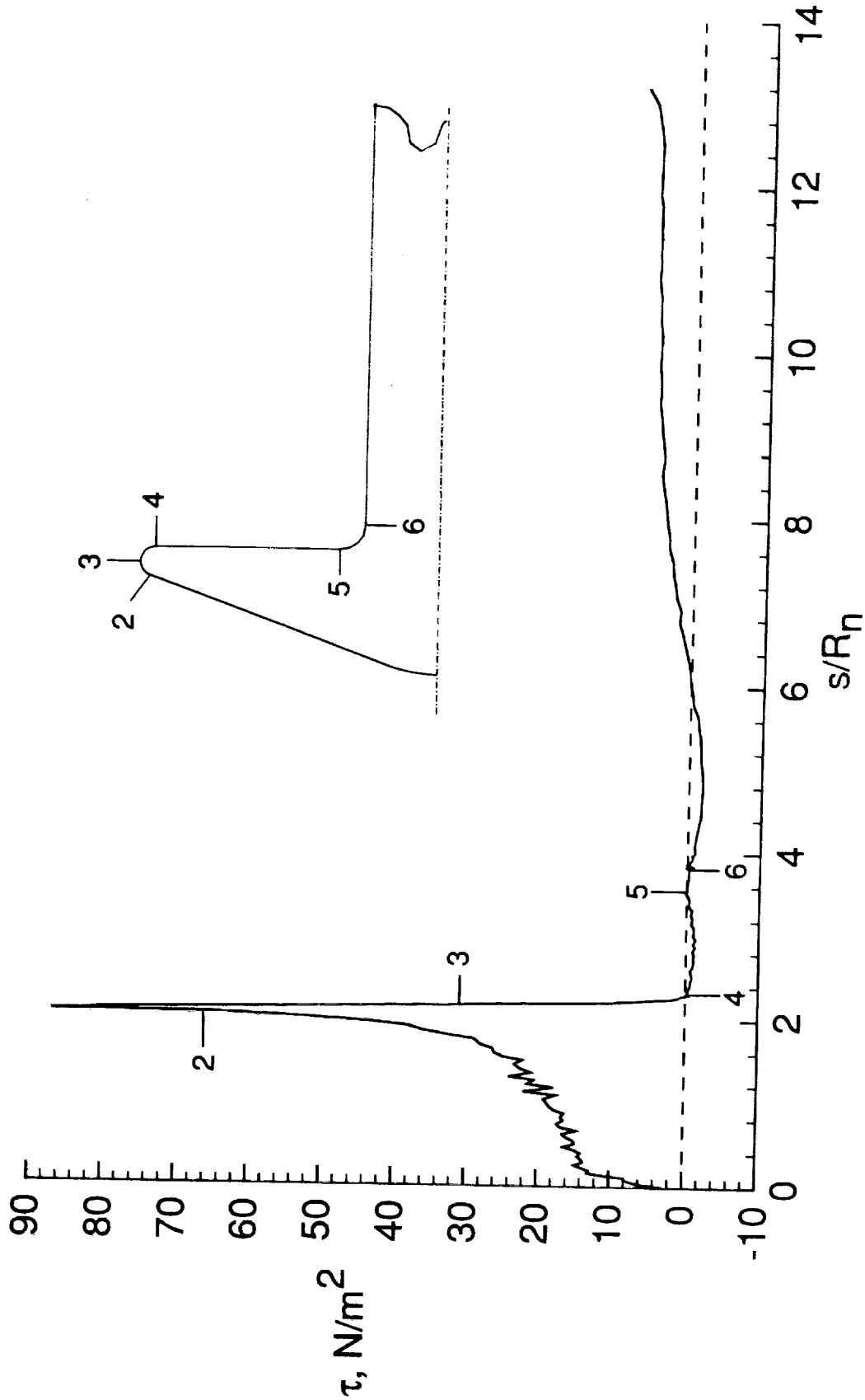

Fig. 5 Skin friction distribution.

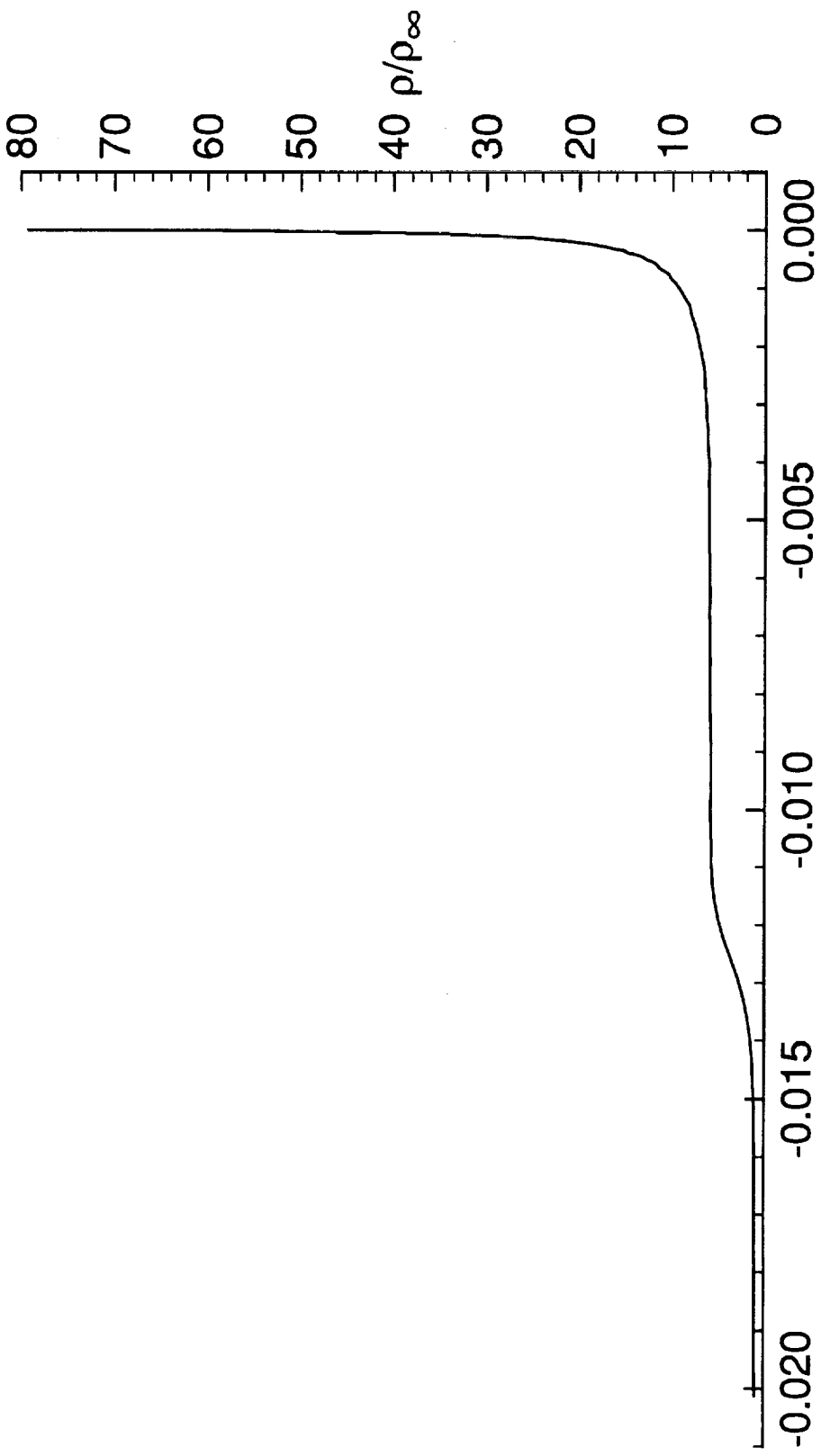

Fig. 6 Stagnation streamline density.

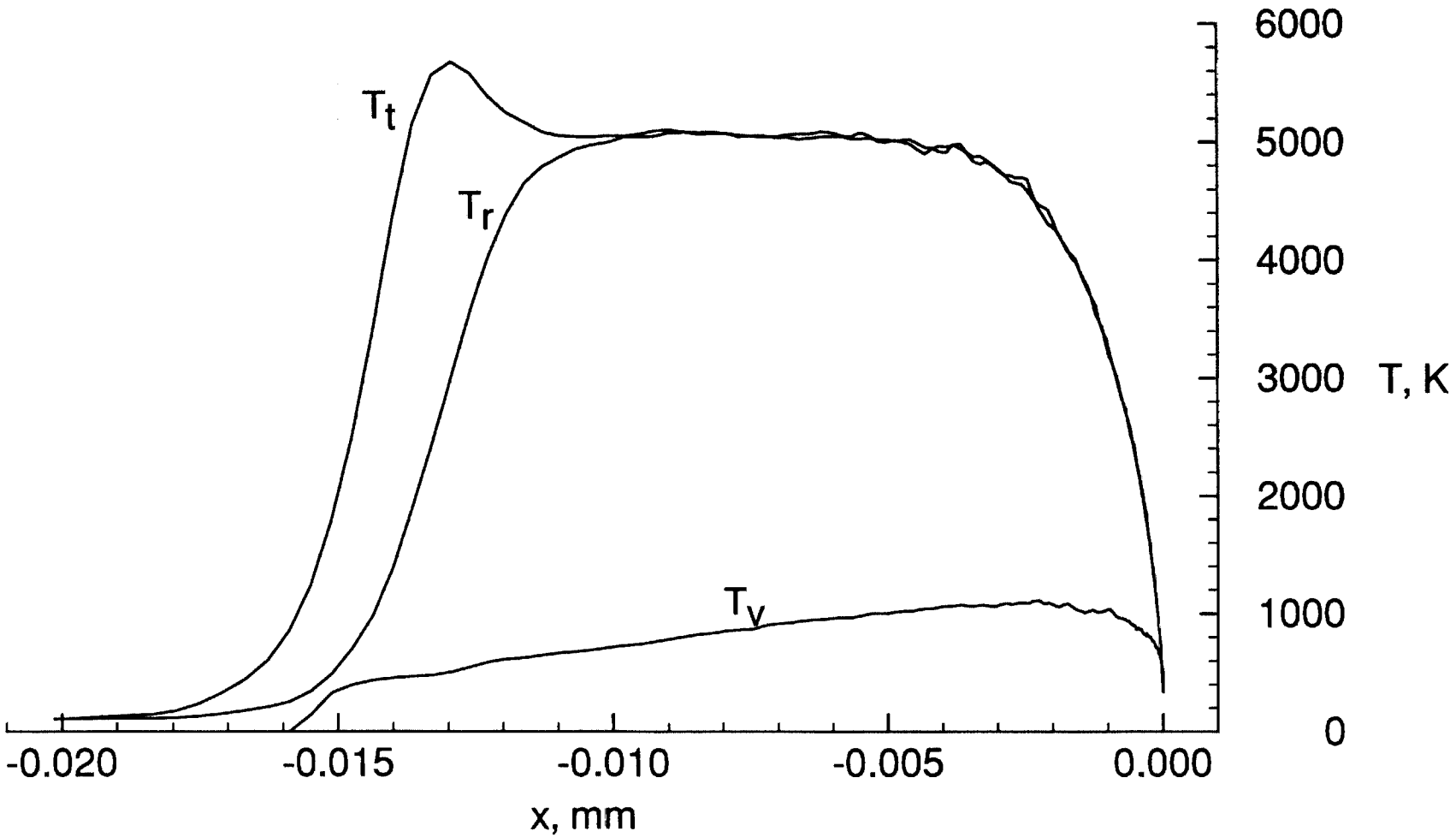

Fig. 7 Stagnation streamline temperature.

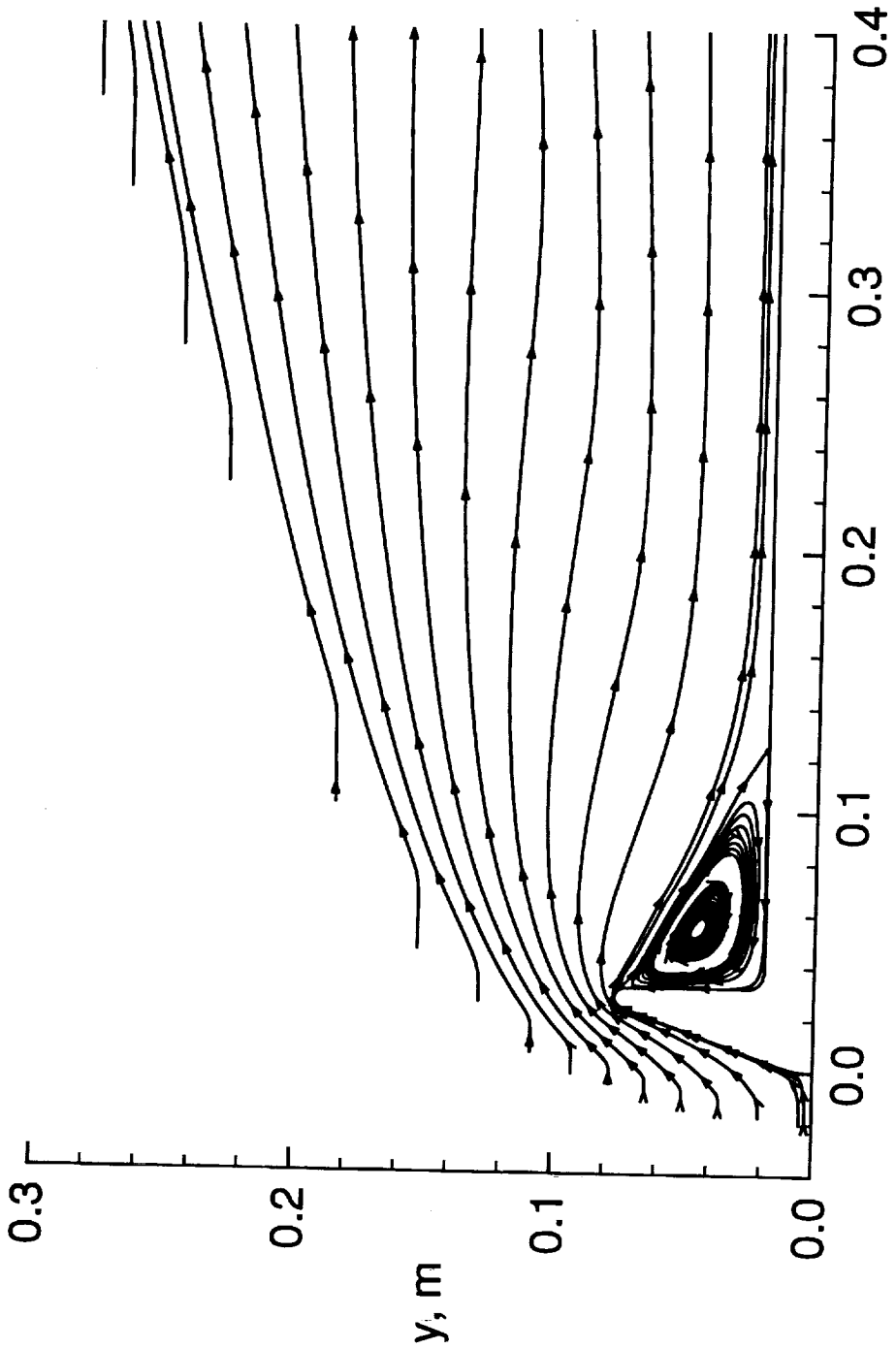

Fig. 8 Streamlines.

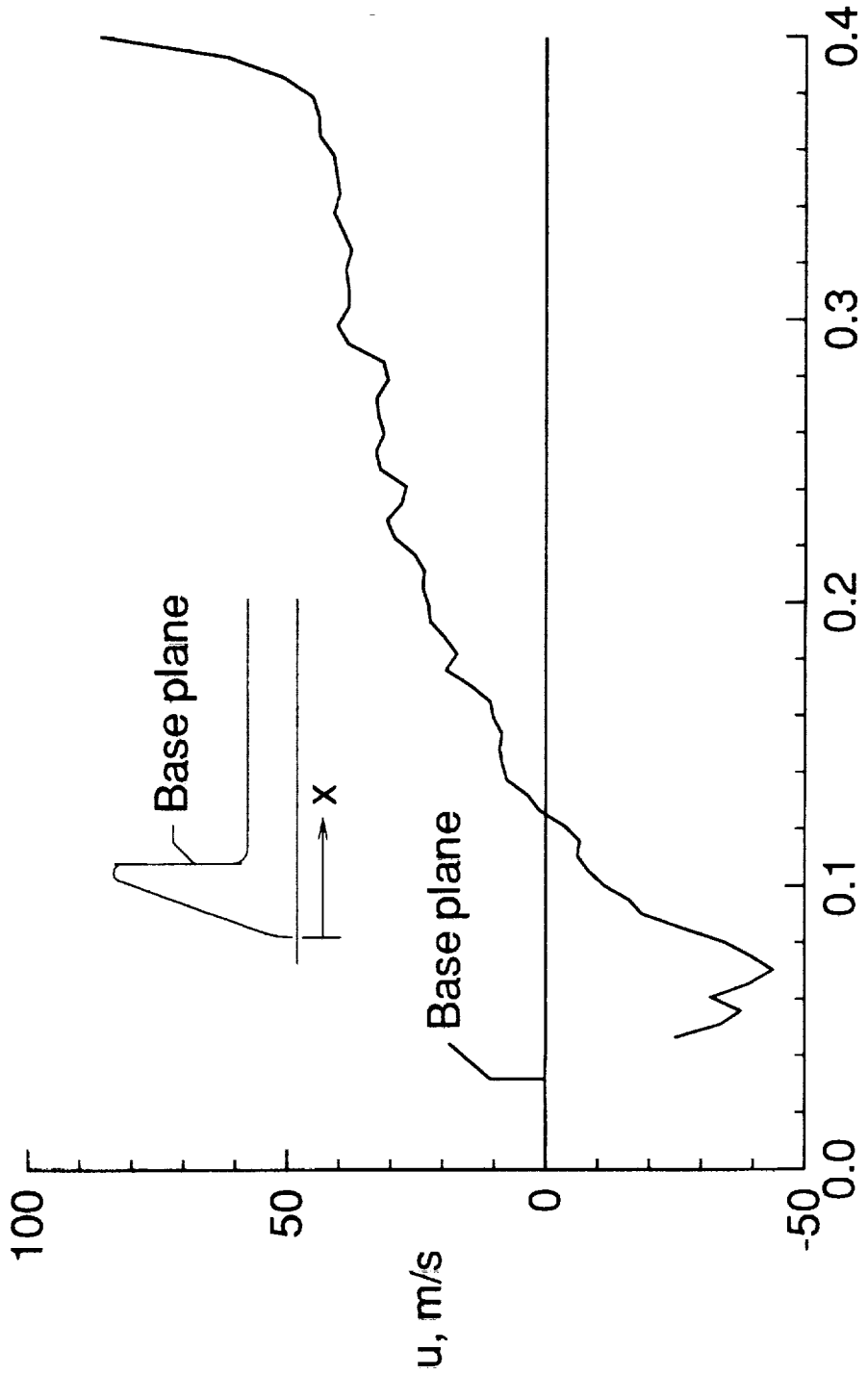

Fig. 9 Tangential velocity.

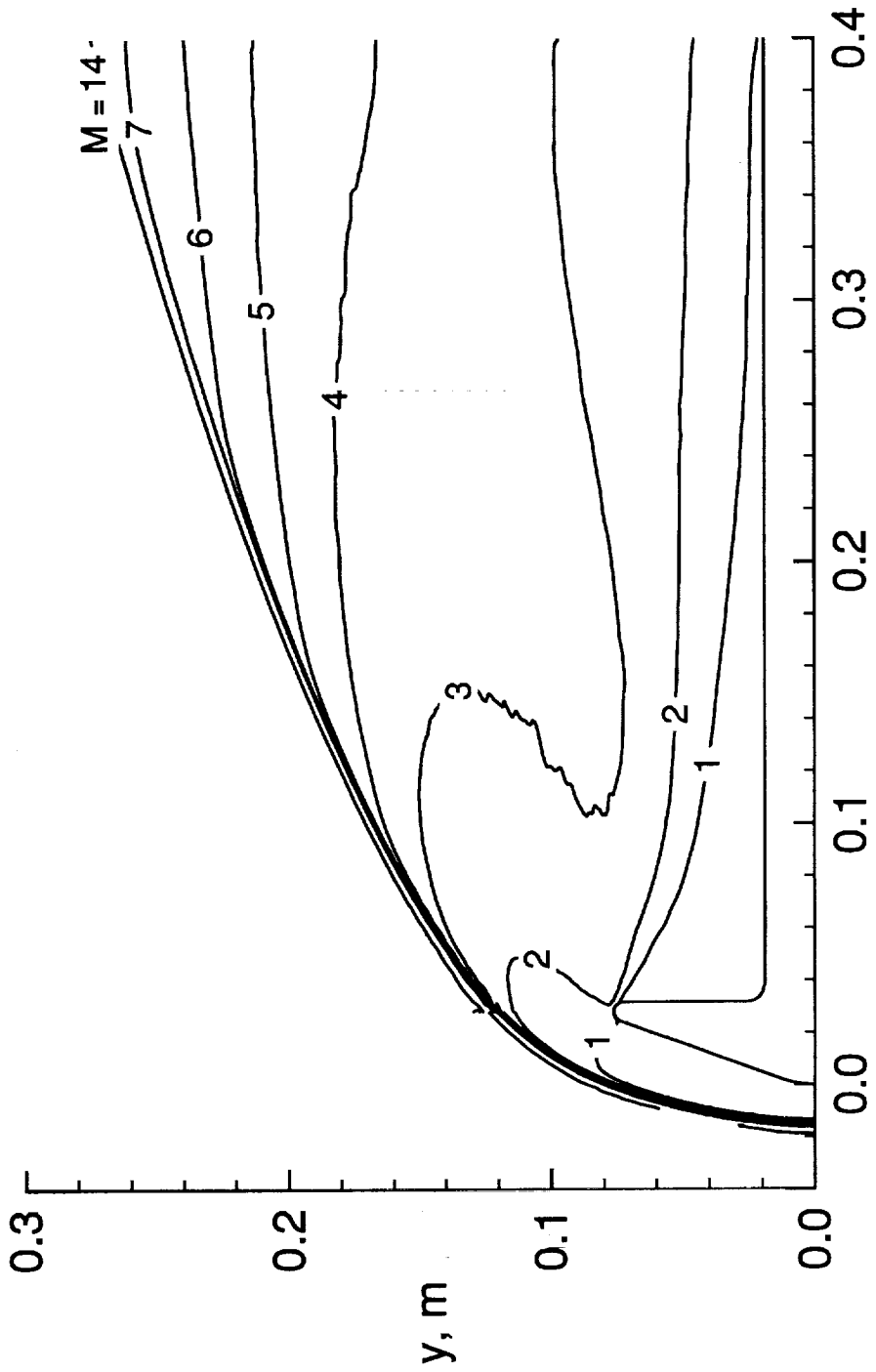

Fig. 10 Mach contours.

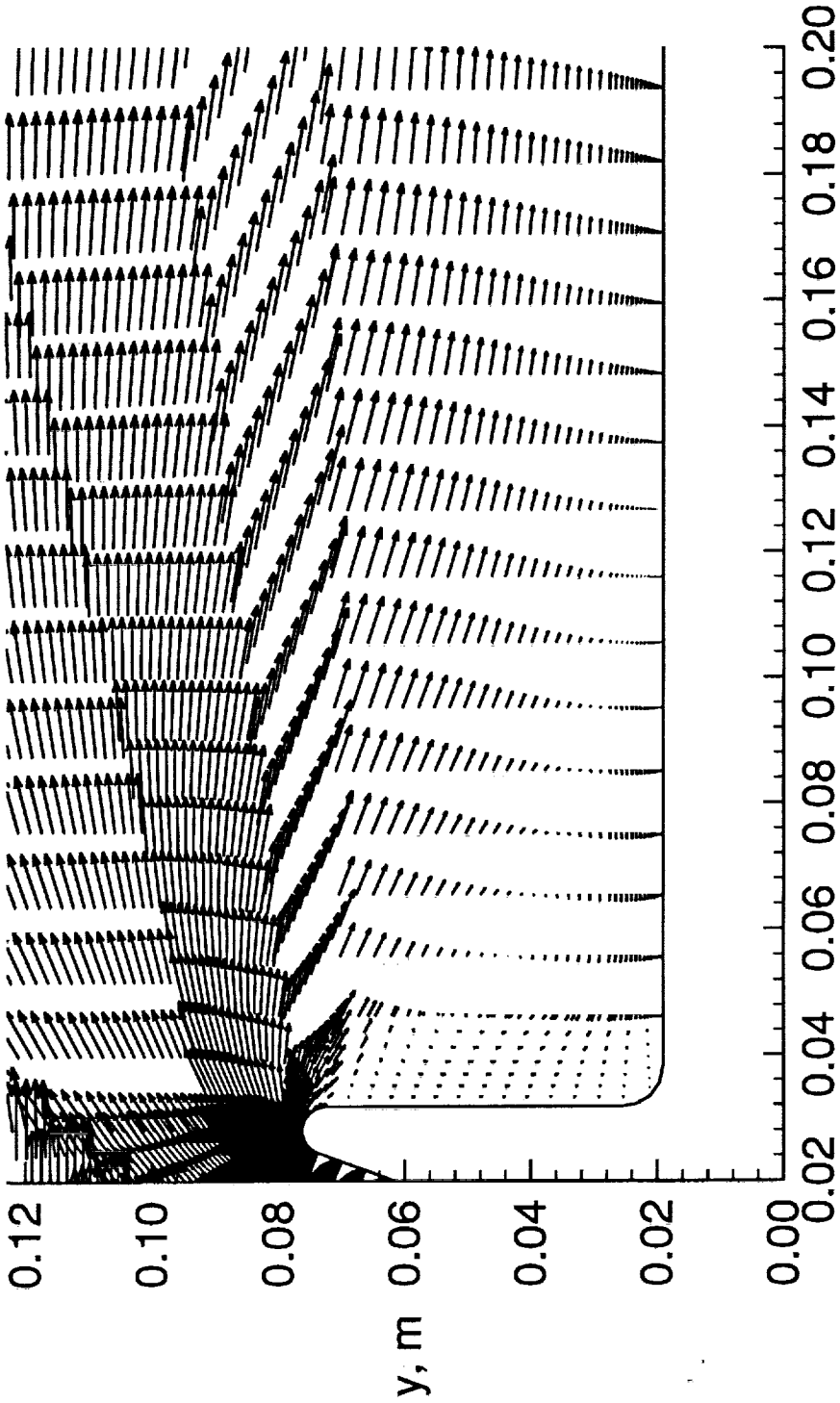

Fig. 11 Velocity vectors in near wake region.

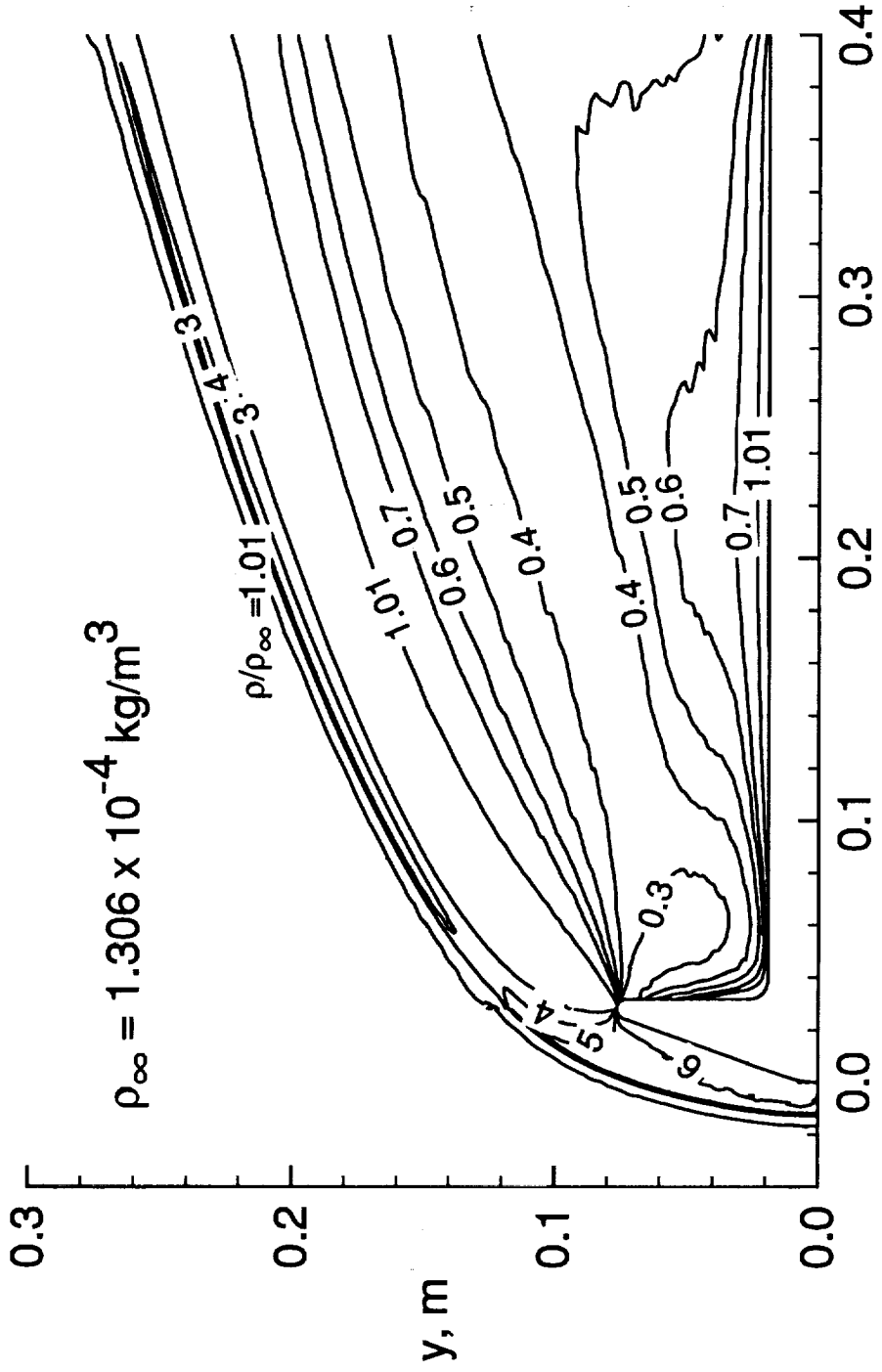

(a) Overall view

Fig. 12 Density contours.

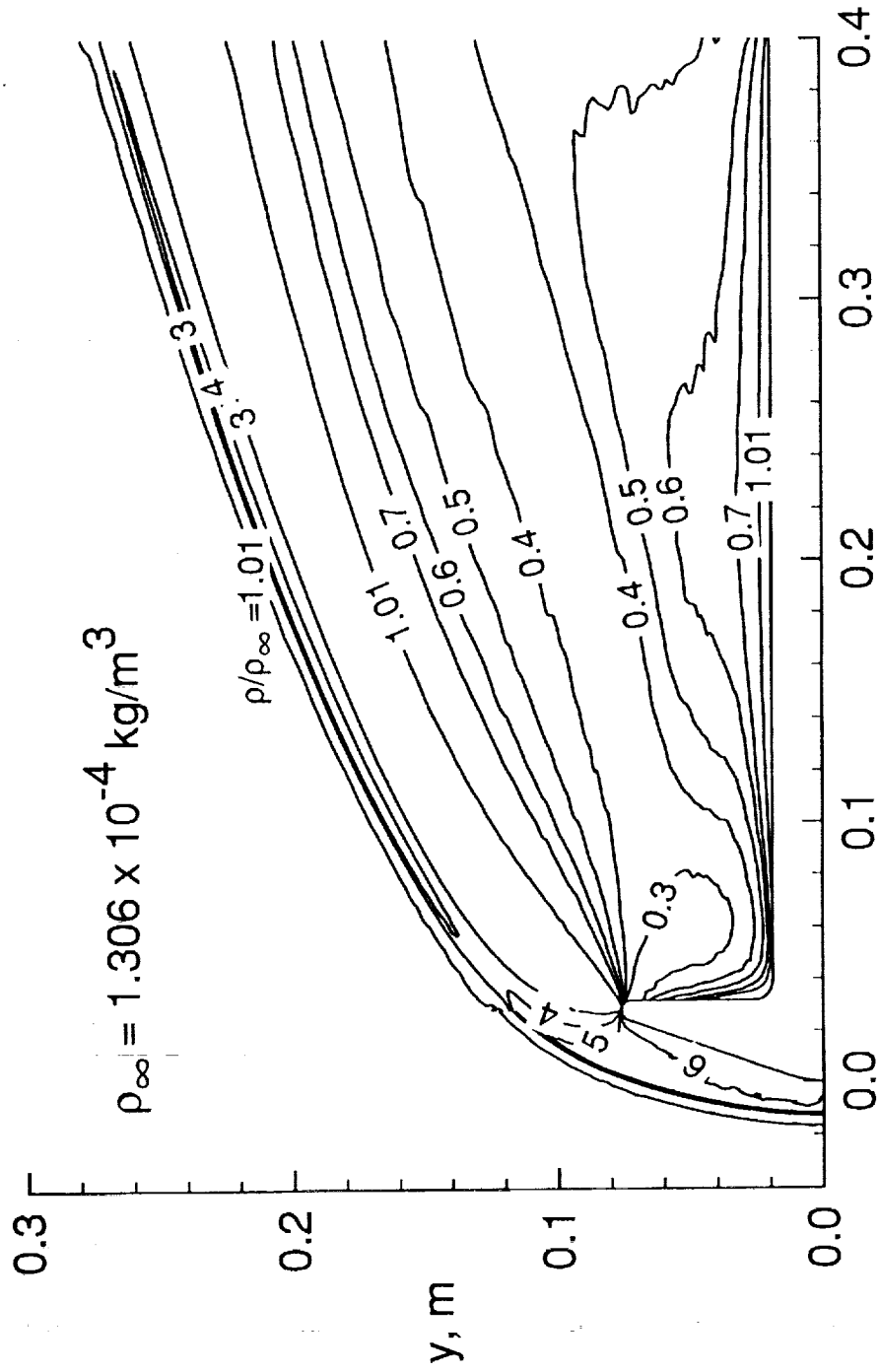

(a) Overall view

Fig. 12 Density contours.

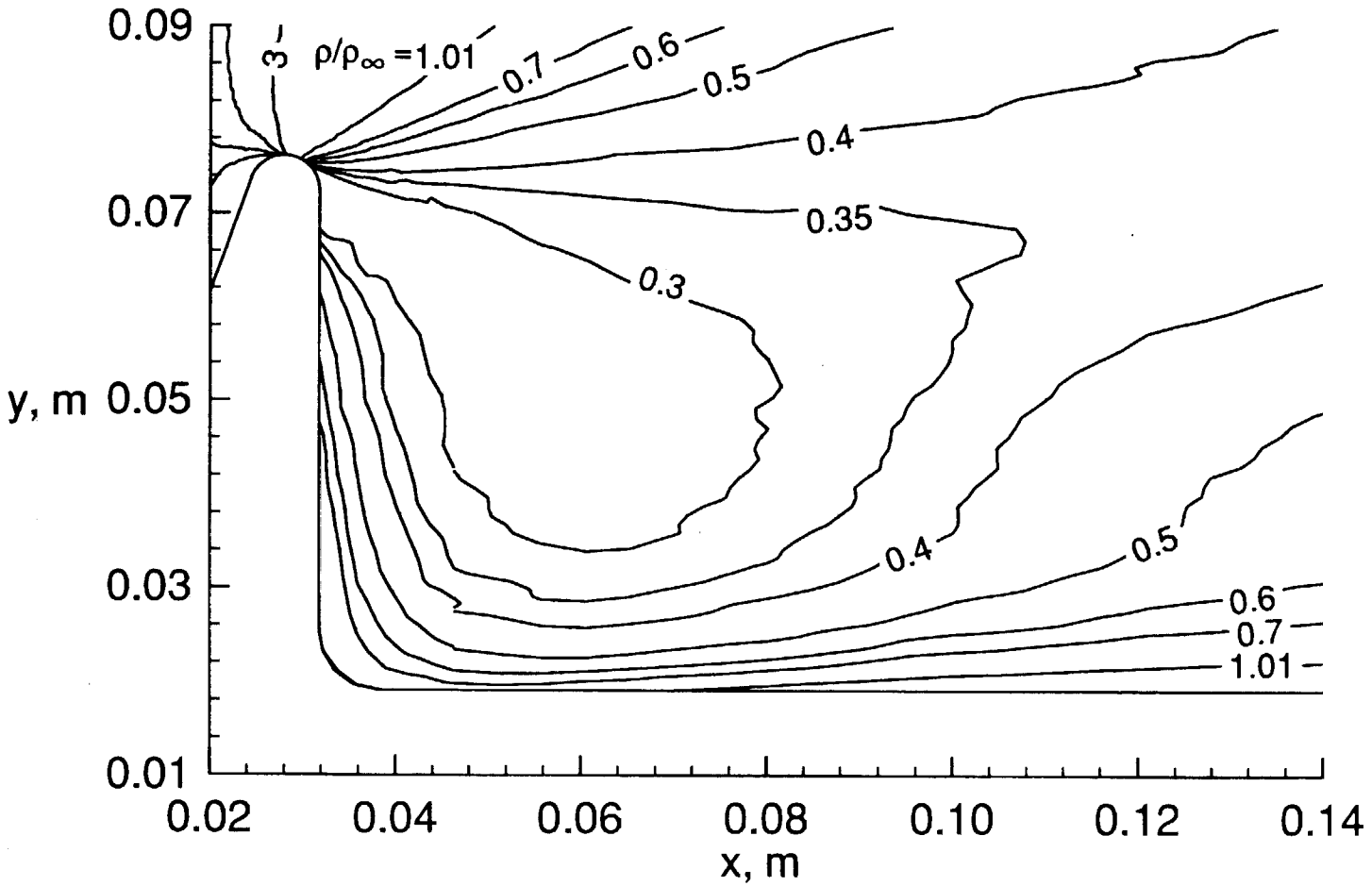

(b) Near wake region

Fig. 12 Concluded.

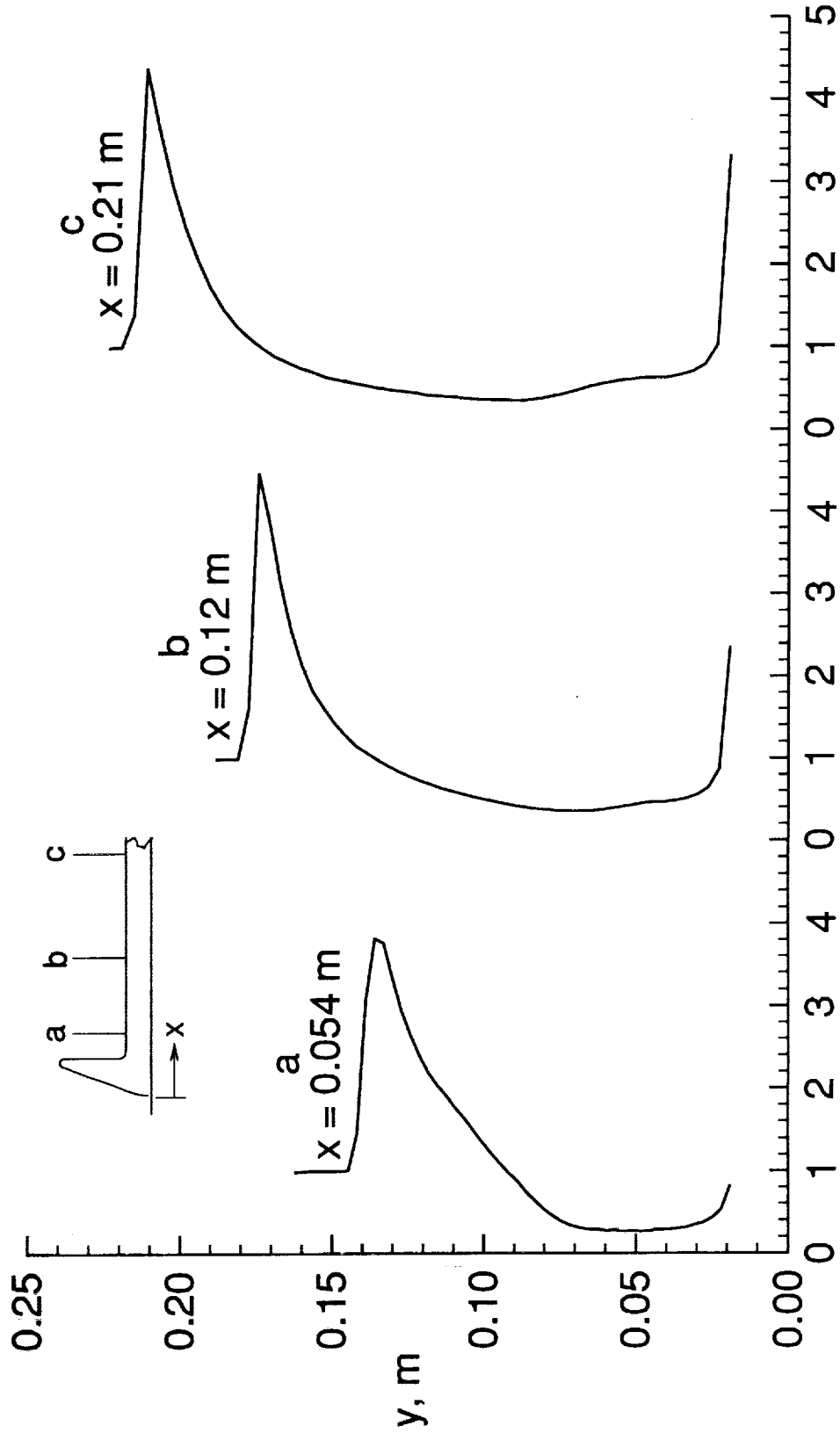

Fig. 13 Wake density profiles.

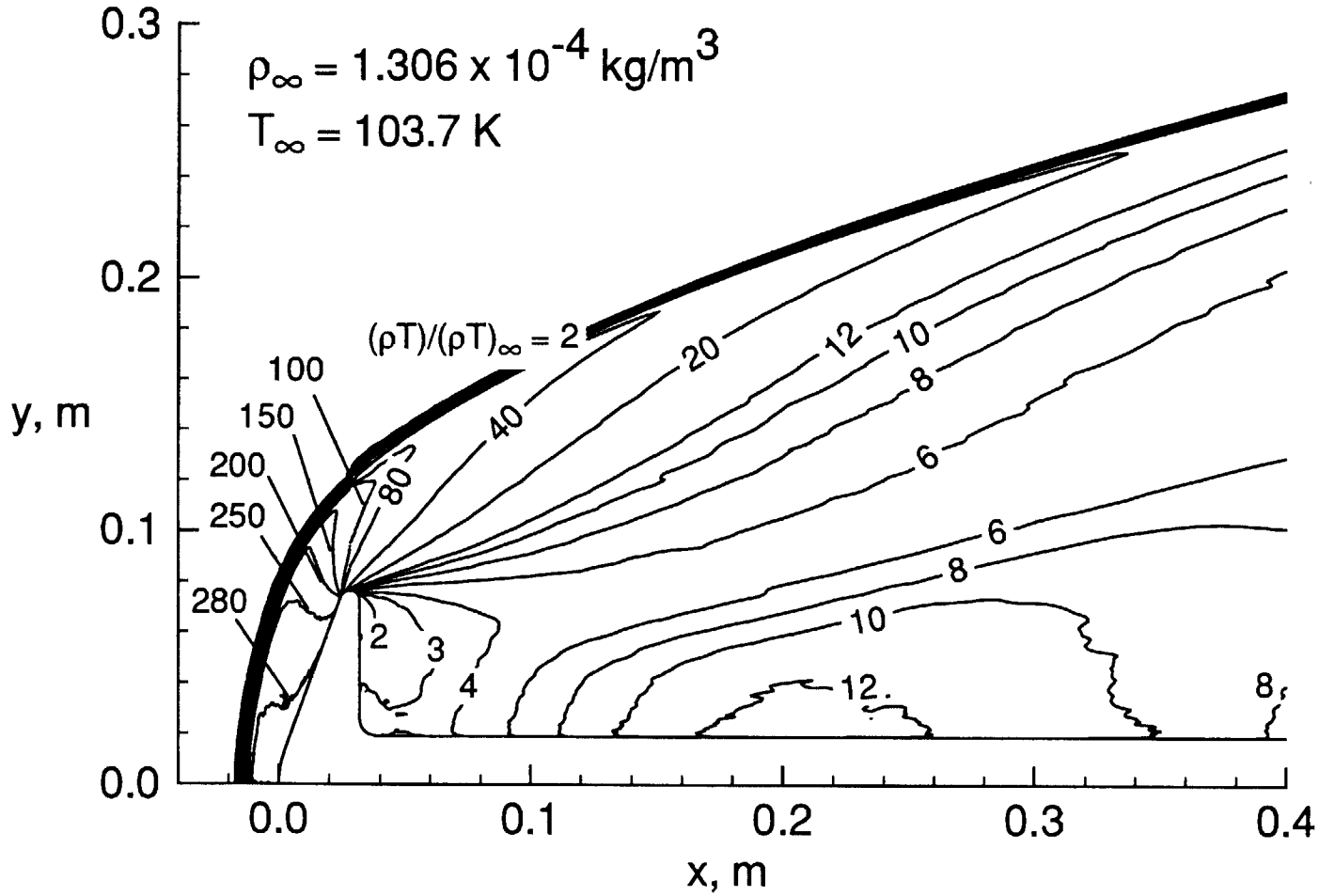

Fig. 14 "Pressure-like" contours.

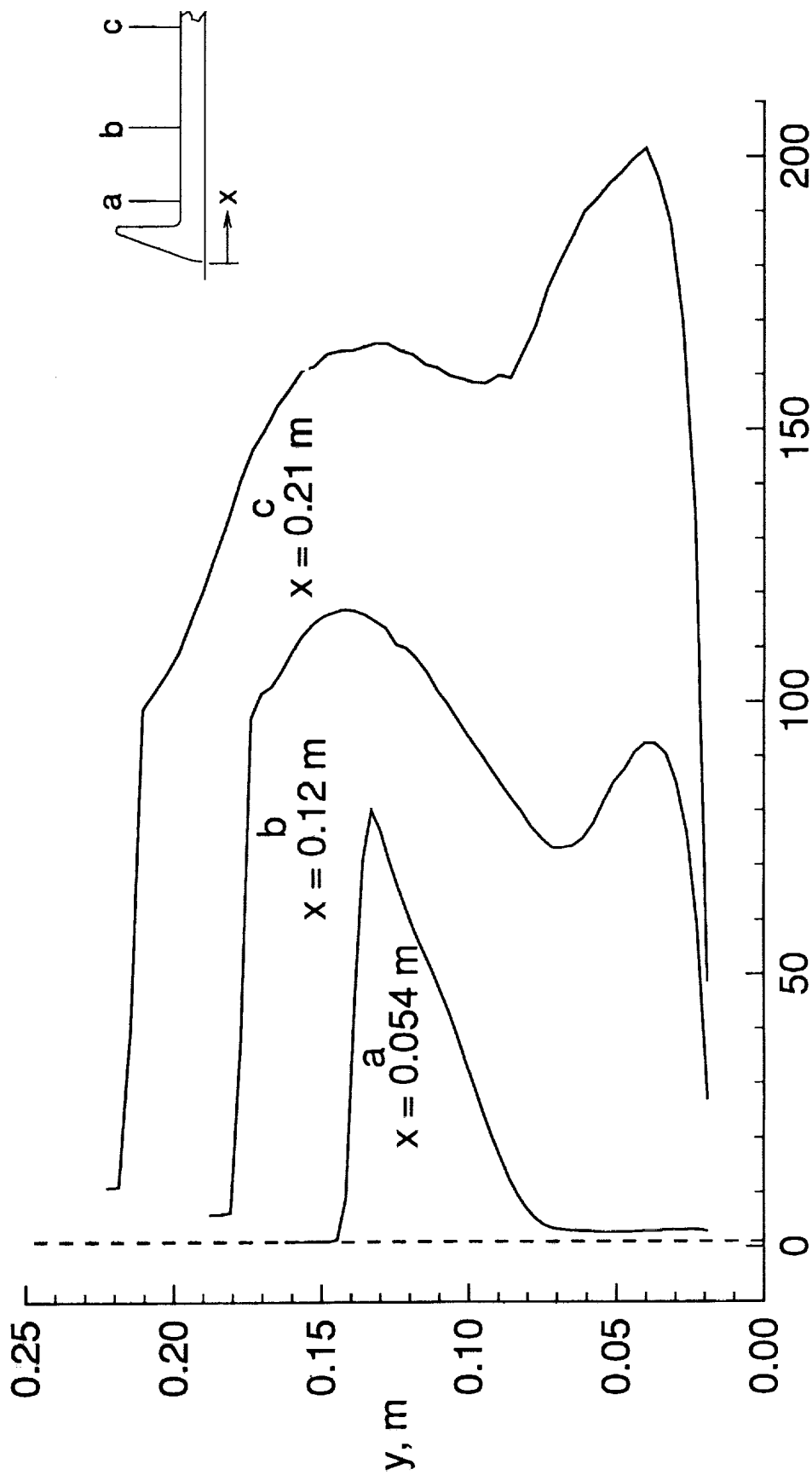

Fig. 15 Wake "pressure-like" profiles.

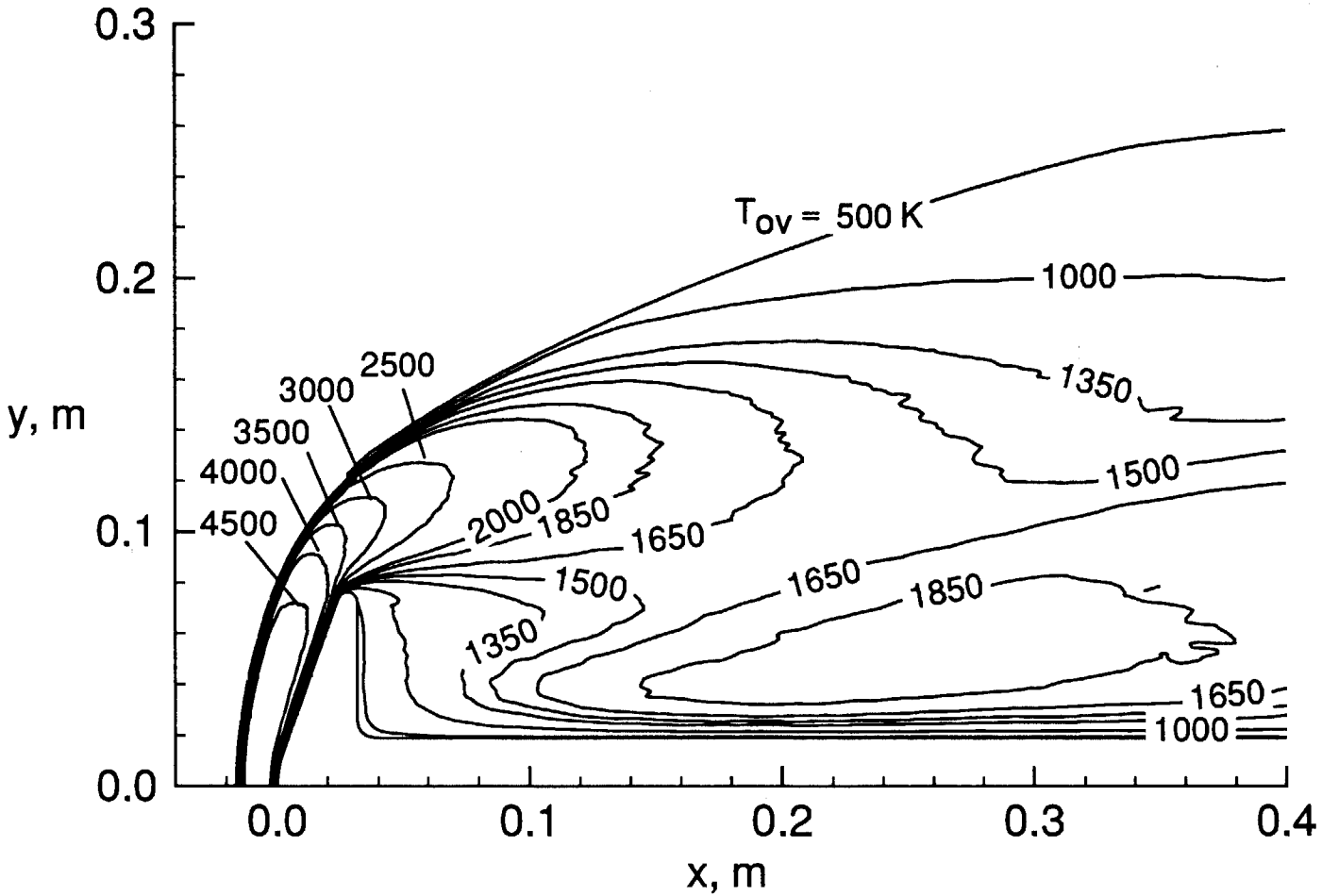

(a) Overall kinetic temperature

Fig. 16 Temperature contours.

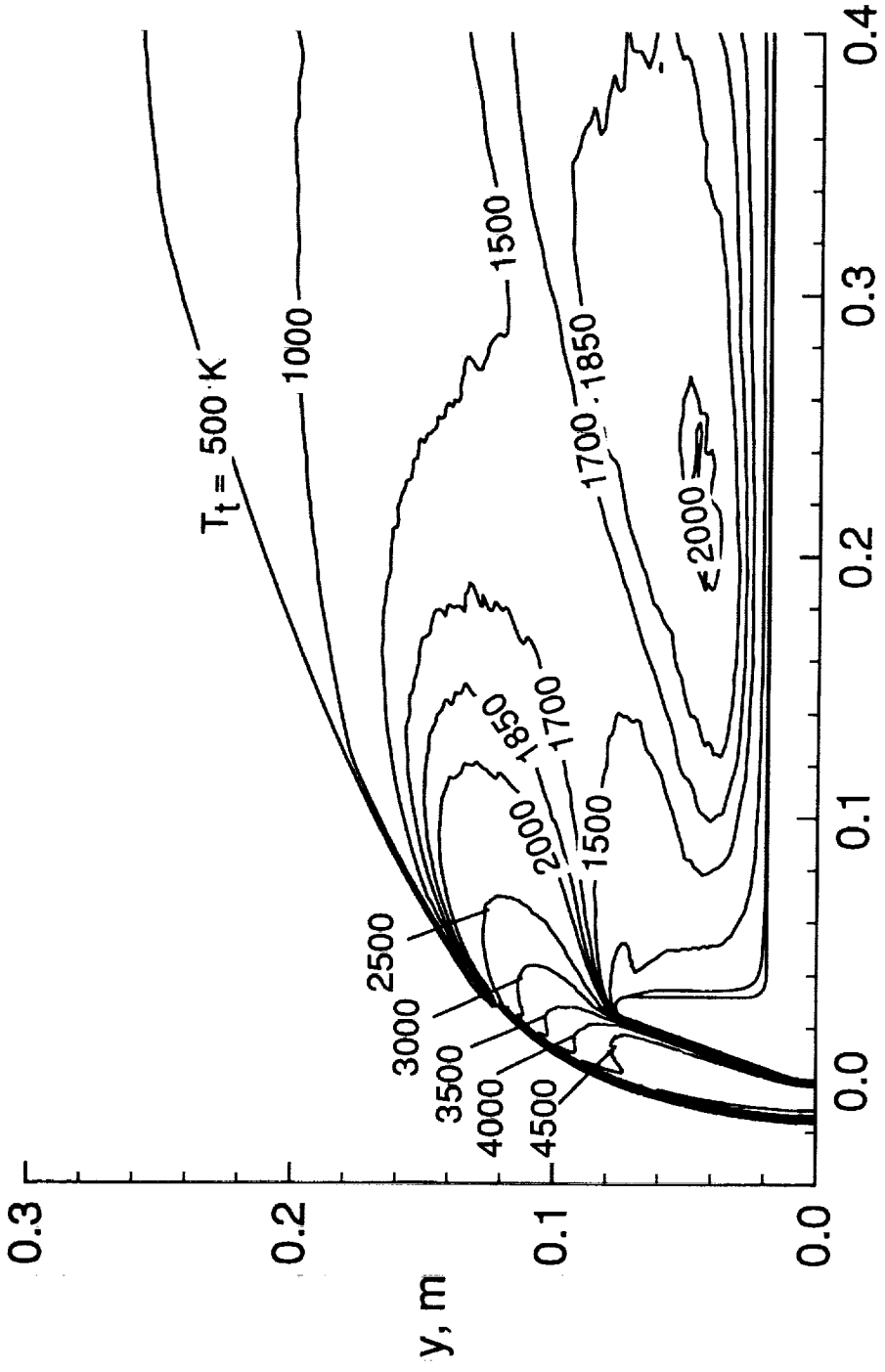

(b) Translational temperature

Fig. 16 Continued.

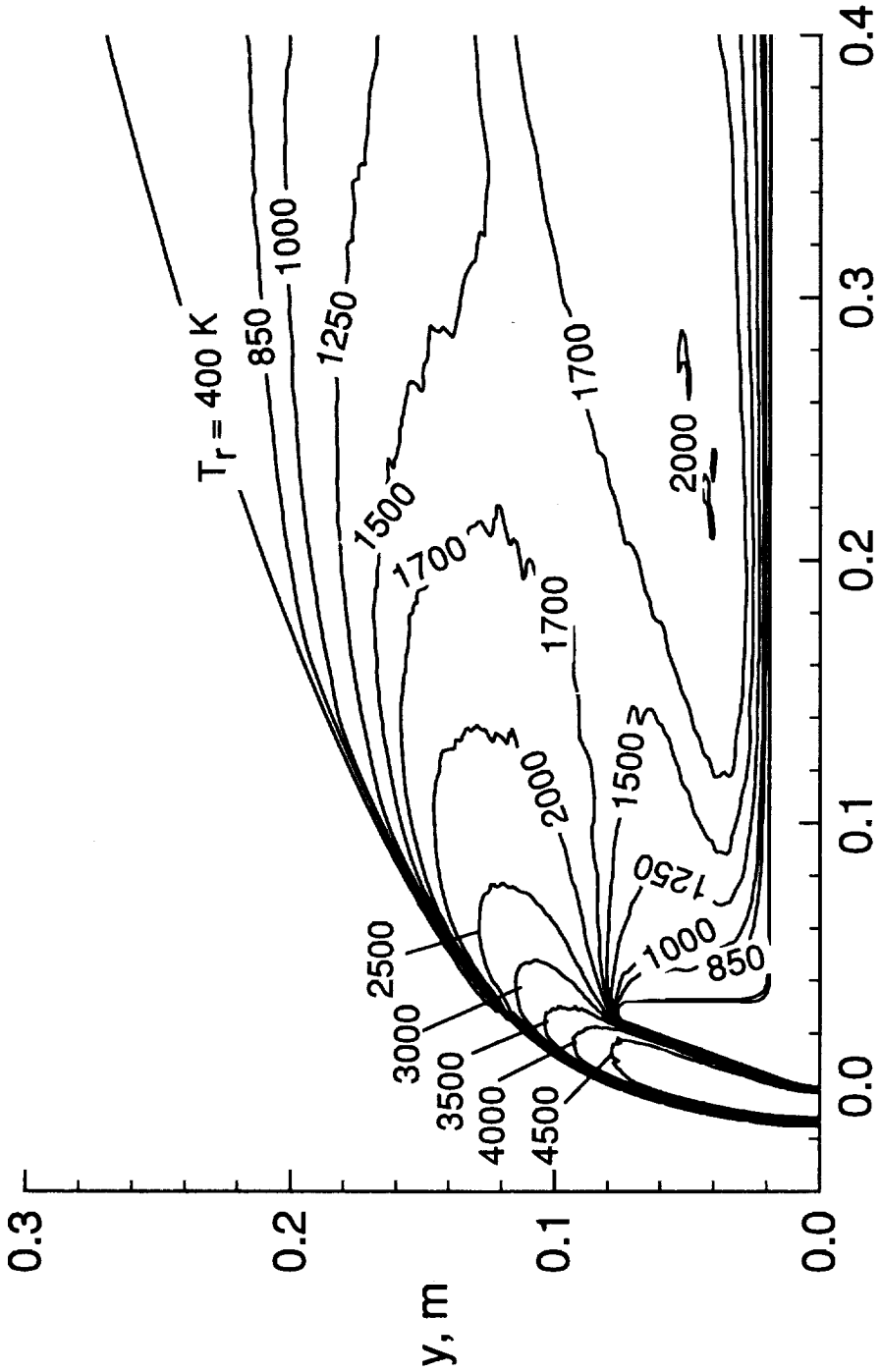

(c) Rotational temperature

Fig. 16 Continued.

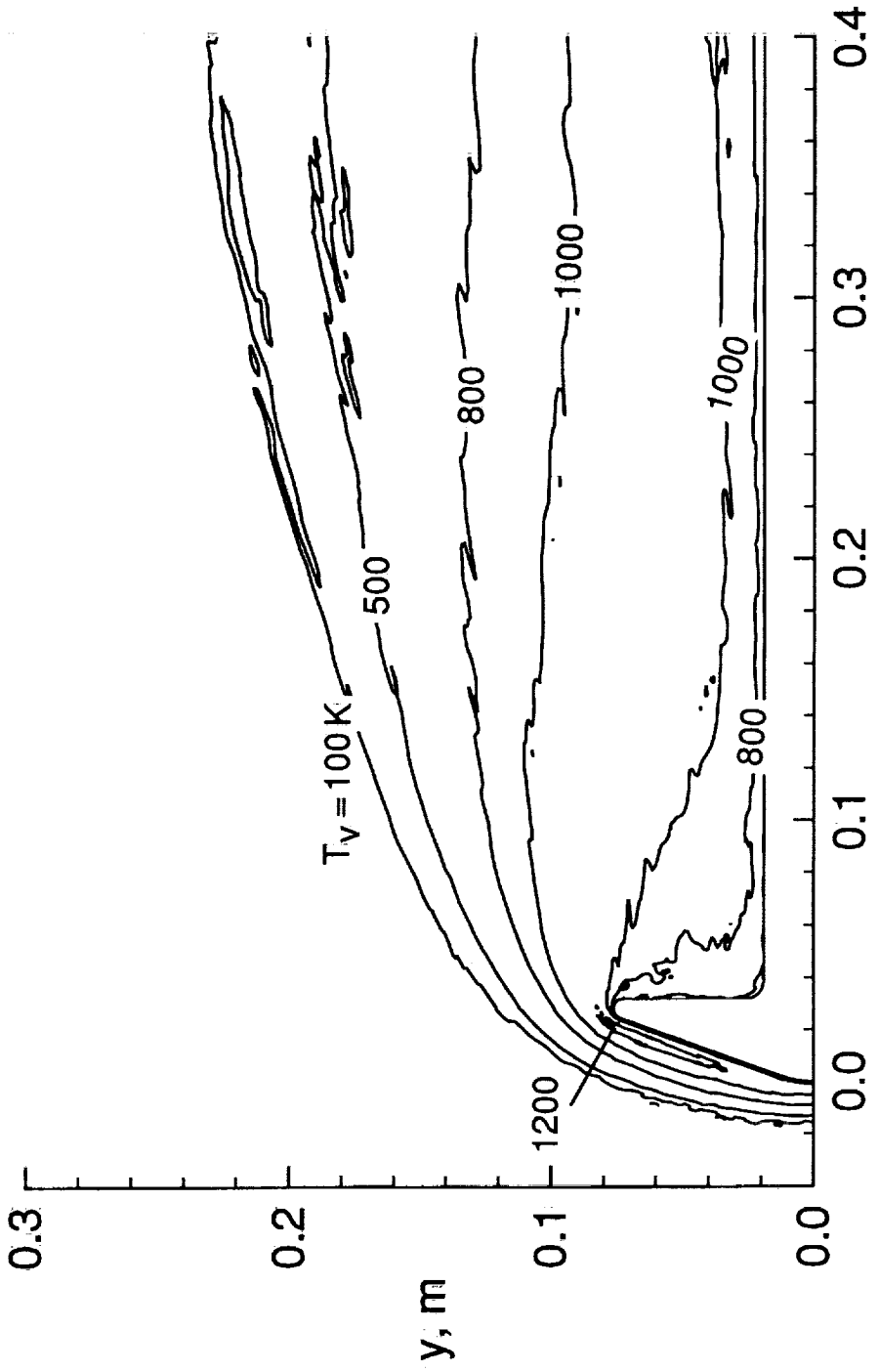

(d) Vibrational temperature

Fig. 16 Concluded.

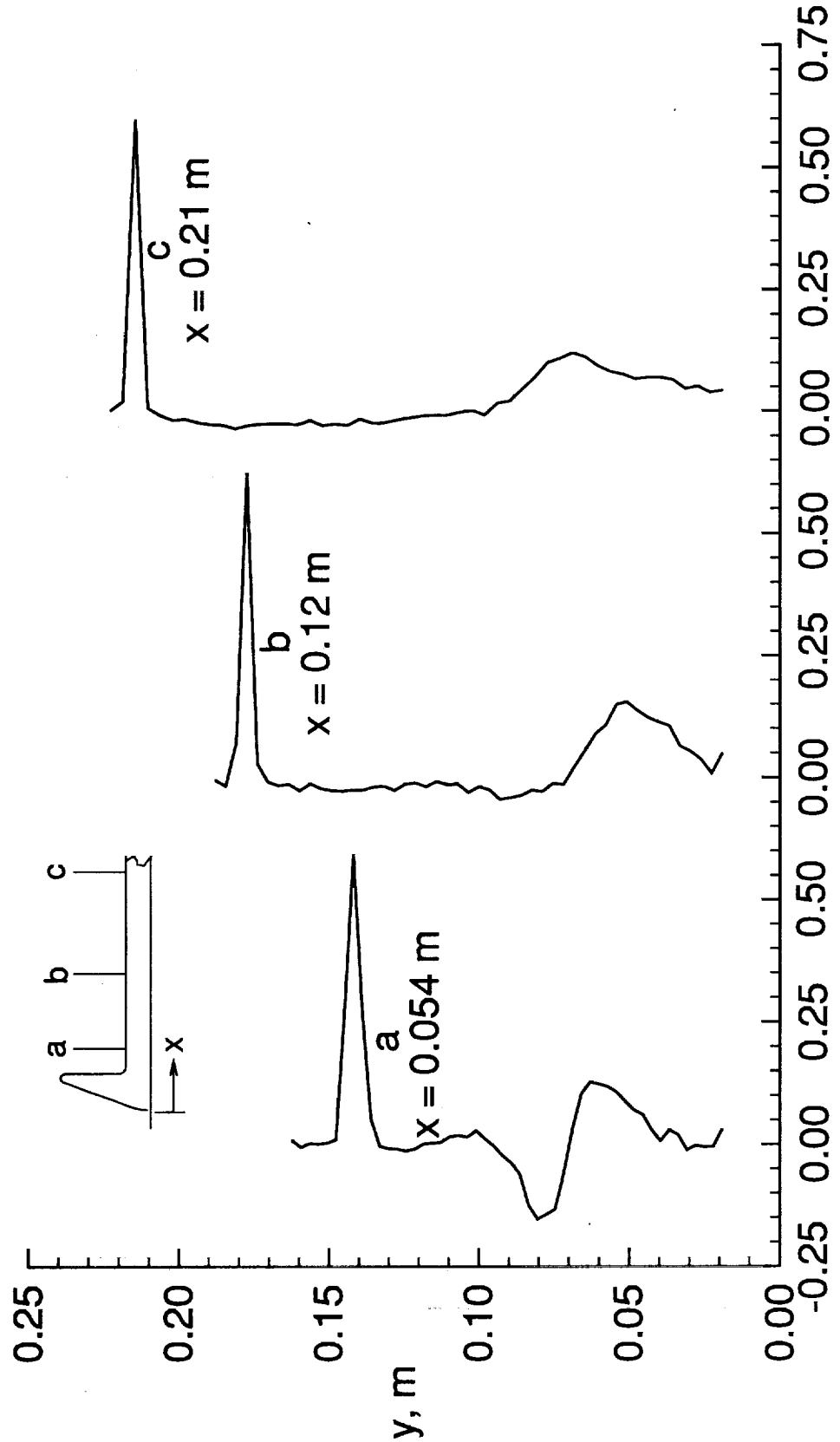

(a) Extent of thermal nonequilibrium.

Fig. 17 Wake profiles.

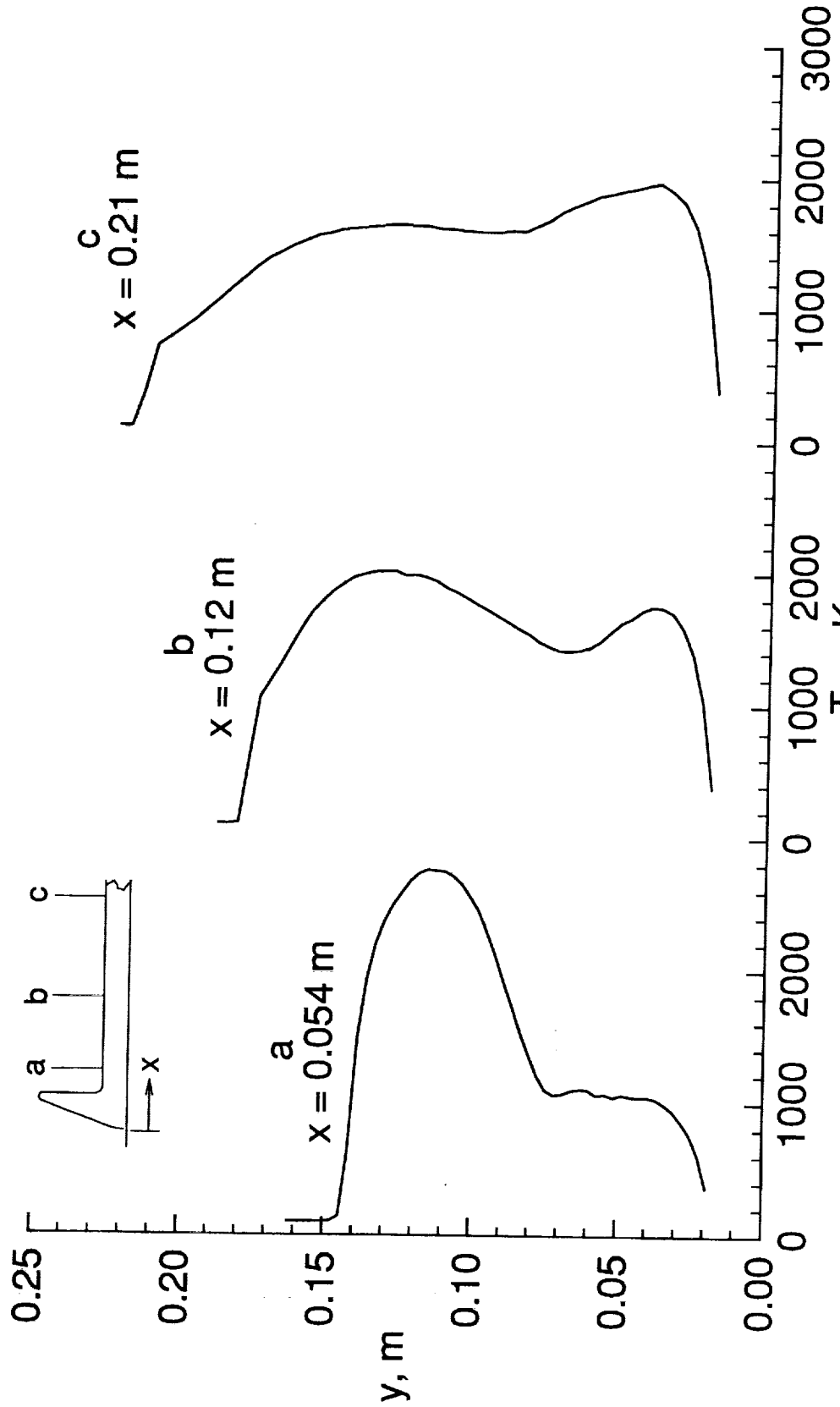

(b) Overall kinetic temperature

Fig. 17 Continued.

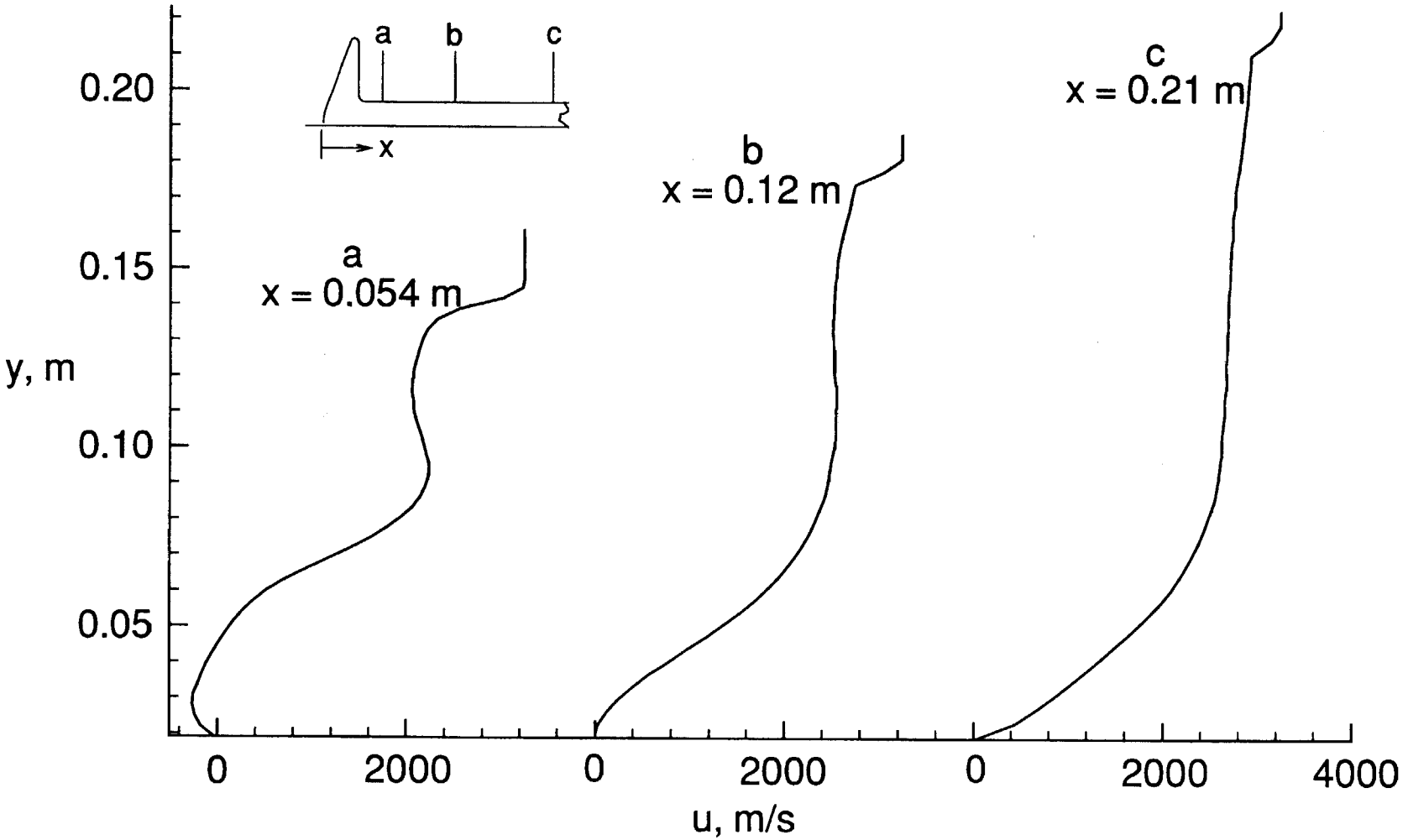

(c) Axial velocity

Fig. 17 Concluded.

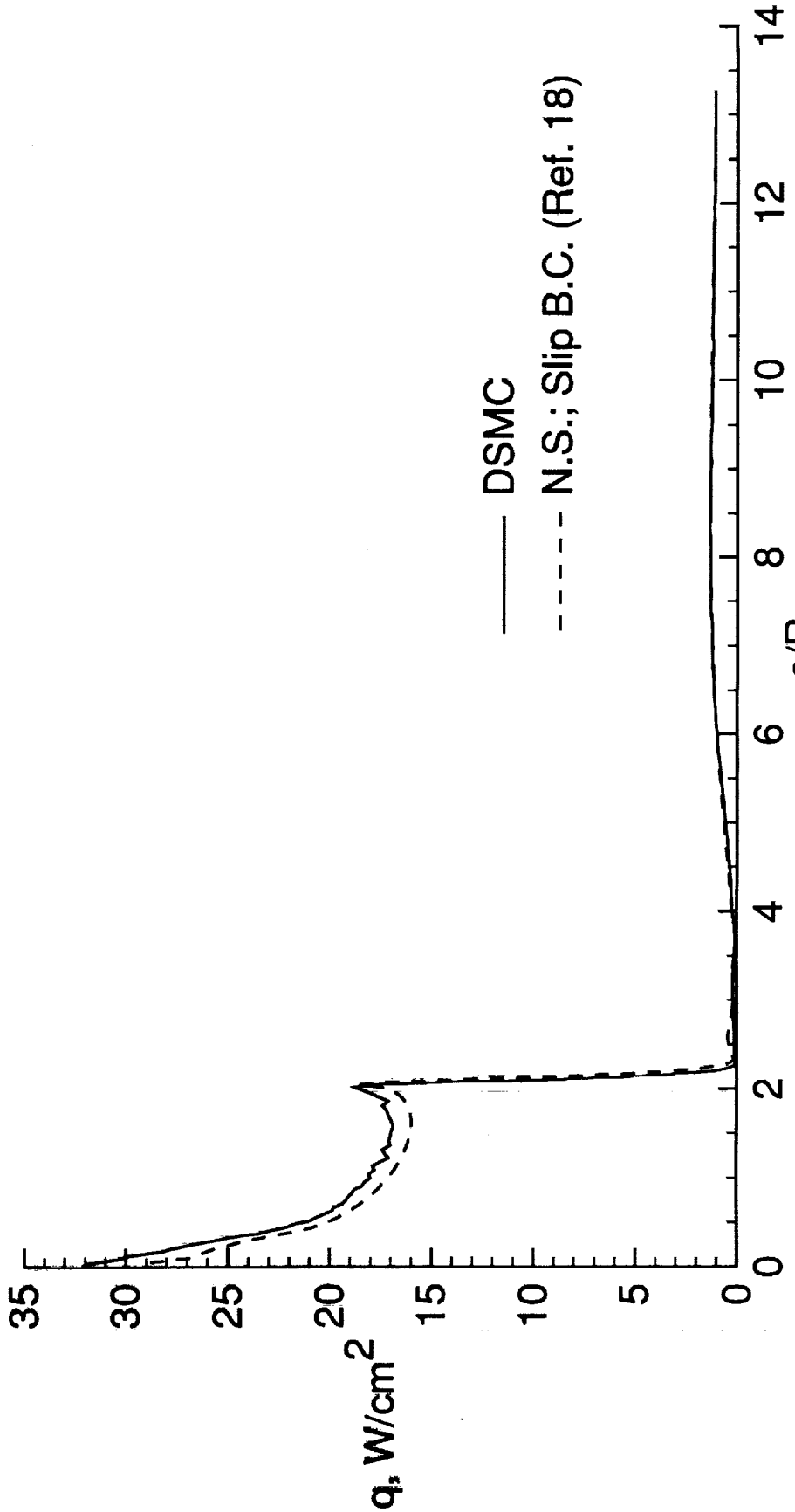

(a) Cartesian plot

Fig. 18 Comparison of calculated surface heating rate.

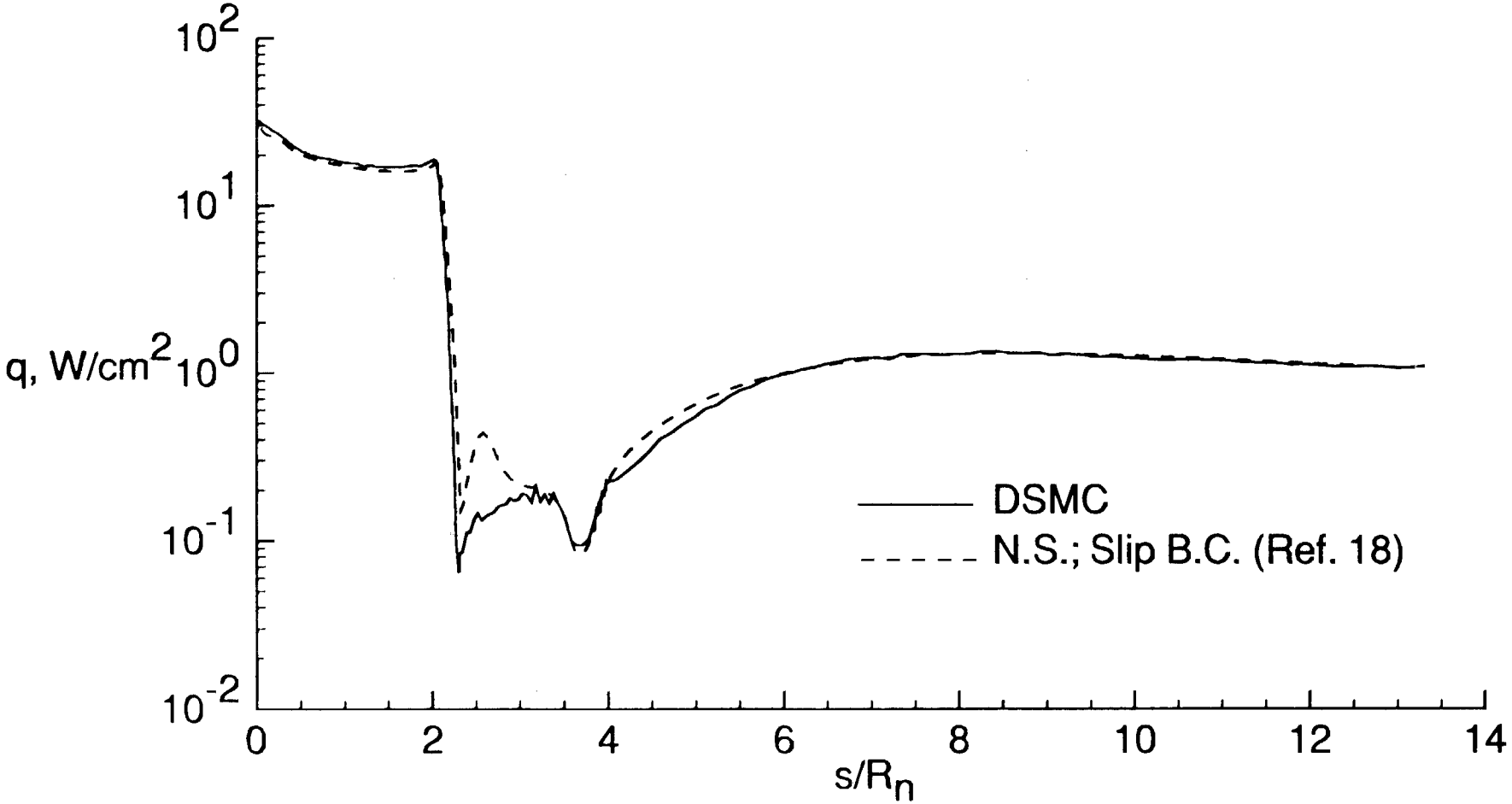

(b) Semilog plot

Fig. 18 Concluded.

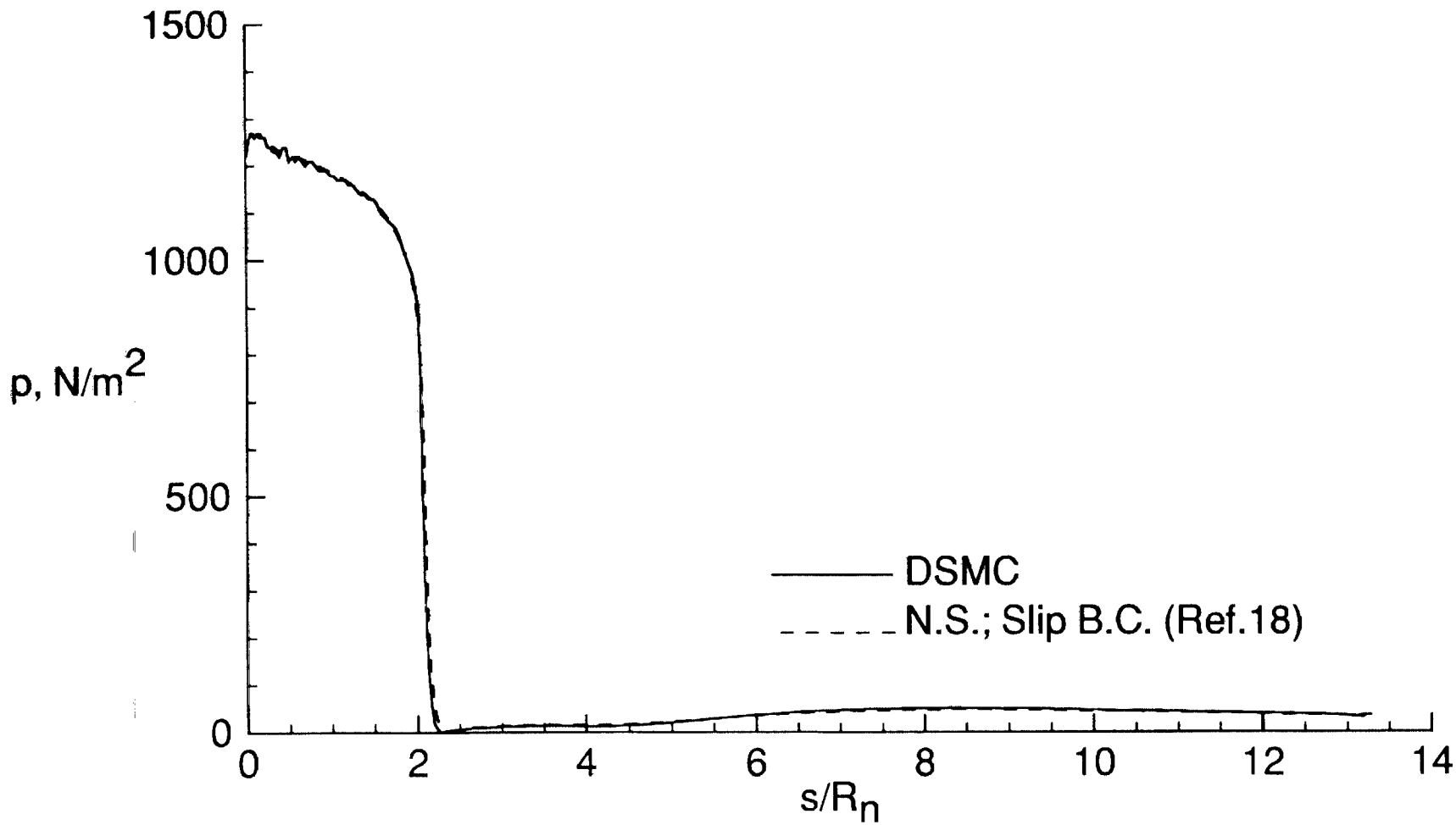

(a) Cartesian plot

Fig. 19 Comparison of calculated surface pressure.

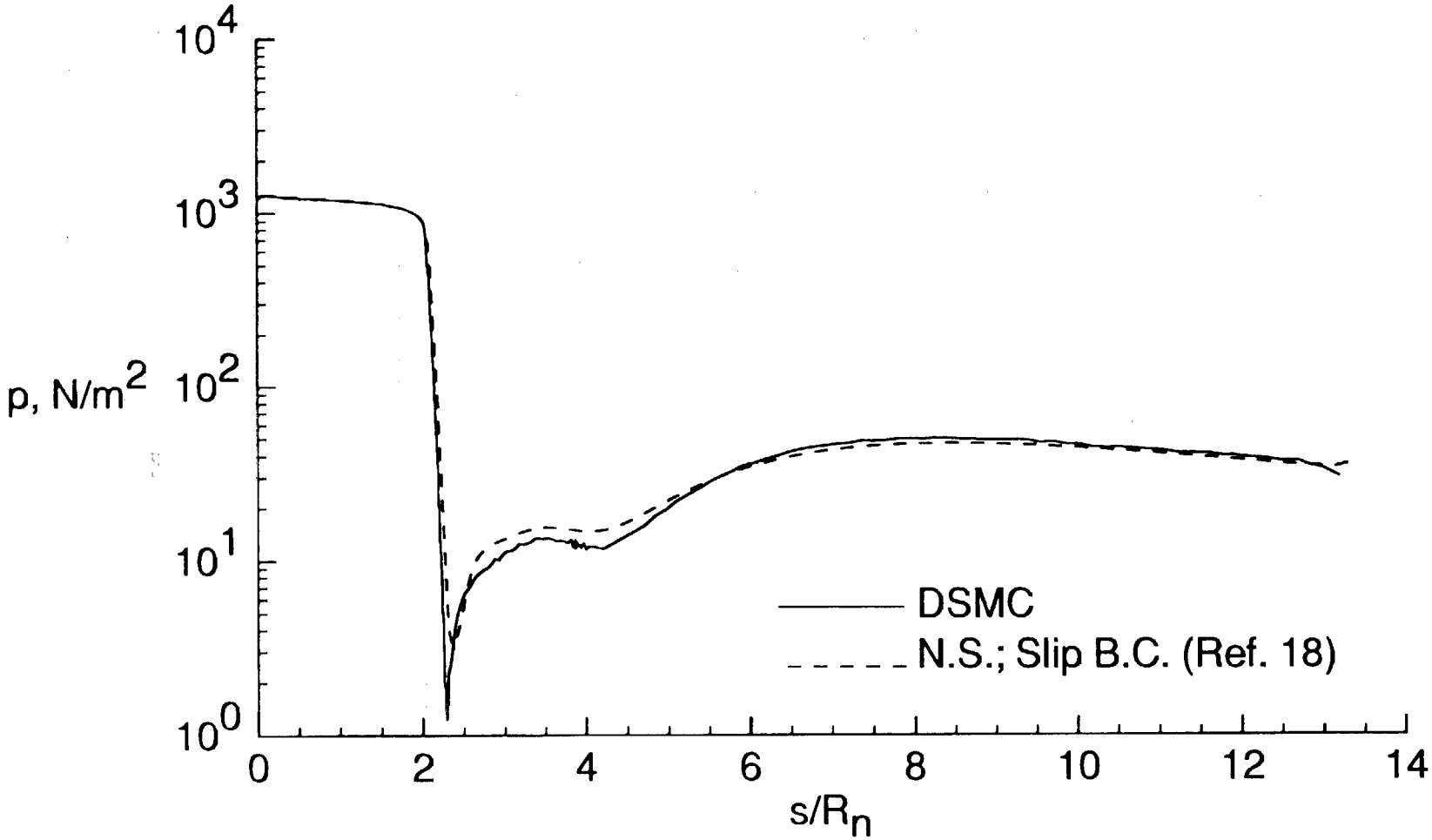

(b) Semilog plot

Fig. 19 Concluded.

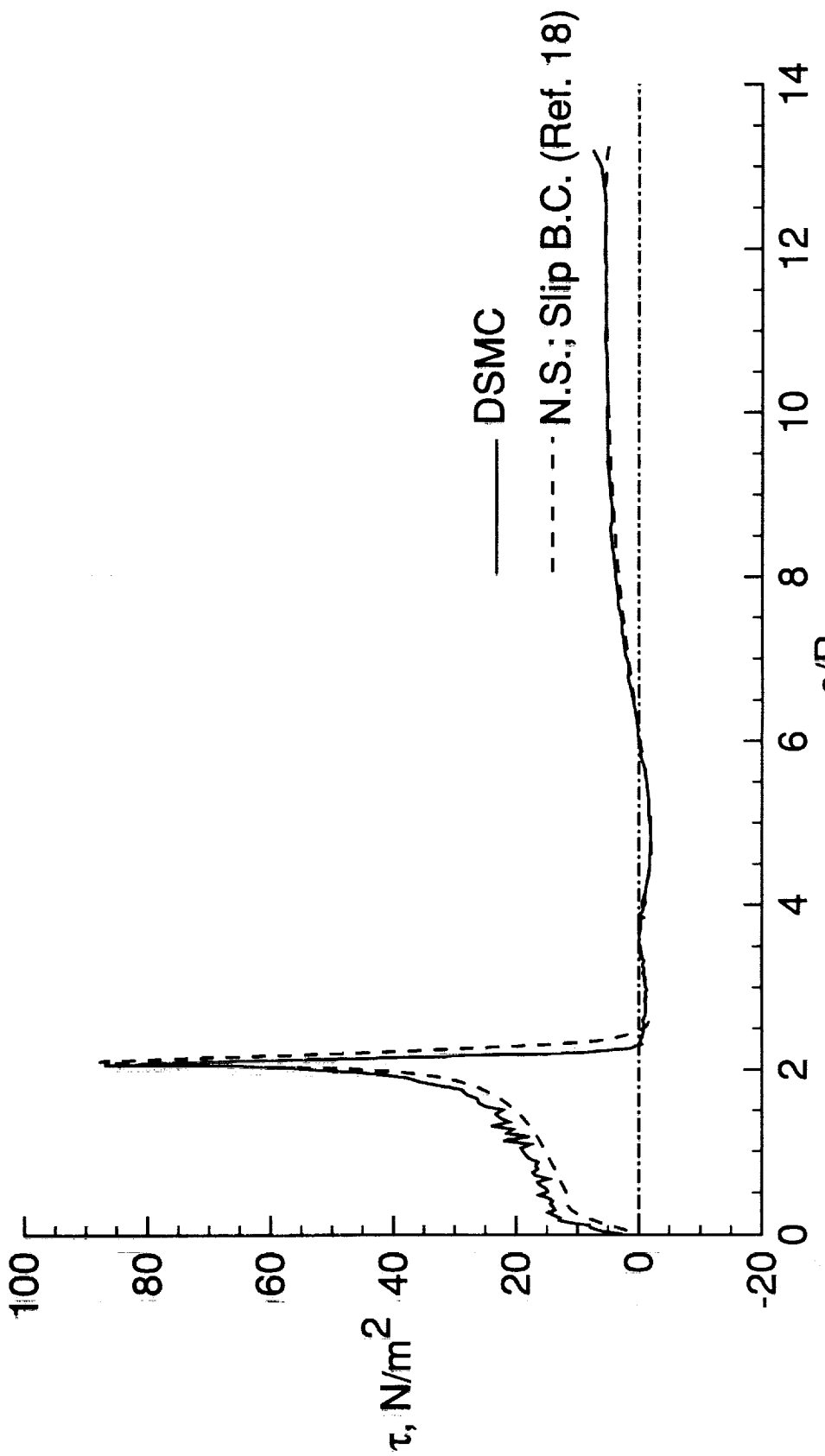

Fig. 20 Comparison of calculated skin friction.

REPORT DOCUMENTATION PAGE

Form Approved
OMB No. 0704-0188

1. AGENCY USE ONLY (*Leave blank*)	2. REPORT DATE	3. REPORT TYPE AND DATES COVERED
	January 1995	Technical Memorandum

4. TITLE AND SUBTITLE
DSMC Calculations for a 70° Blunted Cone at 3.2 km/s in Nitrogen

5. FUNDING NUMBERS
242-80-01-01

6. AUTHOR(S)
James N. Moss, Joseph M. Price, and Virendra K. Dogra

7. PERFORMING ORGANIZATION NAME(S) AND ADDRESS(ES)
NASA Langley Research Center
Hampton, VA 23681-0001

8. PERFORMING ORGANIZATION REPORT NUMBER

9. SPONSORING / MONITORING AGENCY NAME(S) AND ADDRESS(ES)
National Aeronautics and Space Administration
Washington, DC 20546-0001

10. SPONSORING / MONITORING AGENCY REPORT NUMBER
NASA TM-109181

11. SUPPLEMENTARY NOTES
Moss and Price: Langley Research Center, Hampton, VA; Dogra: ViGYAN, Inc., Hampton, VA.

12a. DISTRIBUTION / AVAILABILITY STATEMENT
Unclassified-Unlimited

Subject Category 34

12b. DISTRIBUTION CODE

13. ABSTRACT (*Maximum 200 words*)

Numerical results obtained with the direct simulation Monte Carlo (DSMC) method are presented for Mach 15.6 nitrogen flow about a 70-deg spherically blunted cone at zero incidence. This flow condition is one of several generated in the Large Energy National Shock (LENS) tunnel during tests of a 15.24 cm diameter model with an afterbody sting. The freestream Knudsen number, based on model diameter, is 0.0023. The focus of the DSMC calculations is to characterize the near wake flow under conditions where rarefaction effects may influence afterbody aerothermal loads. This report provides information concerning computational details along with flowfield and surface quantities. Calculations show that the flow enveloping the test model is in thermal nonequilibrium and a sizable vortex develops in the near wake. Along the model baseplane the heating rates are about 0.6 percent of the forebody stagnation value while the maximum heating along the sting is about 4.2 percent of the forebody stagnation value. Comparison of a Navier-Stokes solution with the present calculations show good agreement for surface heating, pressure, and skin friction results.

14. SUBJECT TERMS
direct simulation Monte Carlo (DSMC), blunted cone, hypersonic, near wakes, heat transfer, rarefied

15. NUMBER OF PAGES
53

16. PRICE CODE
A04

17. SECURITY CLASSIFICATION OF REPORT	18. SECURITY CLASSIFICATION OF THIS PAGE	19. SECURITY CLASSIFICATION OF ABSTRACT	20. LIMITATION OF ABSTRACT
Unclassified	Unclassified		